Assessing the Stability of the Motor Networks Recruited During the Bimanual String-Pulling Task Throughout Stroke Recovery

Mikaël Ladouceur

Thesis submitted to the University of Ottawa
in partial fulfillment of the requirements for the
Master of Science in Neuroscience

Department of Cellular and Molecular Medicine
Faculty of Medicine
University of Ottawa

© Mikaël Ladouceur, Ottawa, Canada, 2023

Abstract

In the absence of treatment following strokes, both humans and model organisms demonstrate partial improvements in motor function. Several endogenous mechanisms, such as cortical reorganization, are hypothesized to cause this spontaneous biological recovery. Reorganization of the motor cortex occurs within a time sensitive period and involves both proximal and distal sites of the intact brain. Despite these advancements, whether the same or different cells are used in the reorganized cortex after stroke remains unknown.

In order to identify the motor networks involved in recovery, our lab has begun using the inducible Arc-CreER^{T2}:Rosa-YFP$^{f/f}$ mice. In conjunction with the bimanual string-pulling task, this inducible model allows for the labelling of active cells throughout stroke recovery; either pre, 2 days post-stroke (dps) and 2 weeks post-stroke (wps). Behavioural deficits on the string-pull task were observed at 2 dps and accompanied by a decrease in active cells in the ipsilesional secondary motor (M2) cortex of stroke mice. By 2 wps, stroke mice had partial recovery of motor function with no differences in active cells in the ipsilesional M2. Interestingly, ~40% of cell in the motor cortex of sham and stroke mice were activated more than once while performing the string-pull task until 2 wps. Deeplabcut kinematic analysis of the string-pull task was also unable to identify differences in motor performance between stroke and sham mice. In addition, irrelevant of stroke injuries, only 60% of cells co-expressed the pan-neuronal marker NeuN after surgeries. Together these findings suggest that 40% of cells are reactivated up to 2 weeks post-stroke during the performance of a motor task, despite the acute decreases in active cells in the ipsilesional M2 of stroke mice. DeepLabCut kinematic results also highlight the need to redefine kinematic outcomes to better assess the full spectrum of stroke deficits.

Table of content

Abstract……..……..II

List of figures…….…….V

List of abbreviations……..……..……..VI

Acknowledgements……..…….,,,……VIII

1. Introduction

1.1 Stroke…….1

1.2 Spontaneous Biological Recovery Following Stroke……...…….3

1.3 Cortical Reorganization in Humans…….….4

1.4 Cortical Reorganization in Preclinical Models…….……....6

1.5 Using a TRAP Model to Detect Cortical Reorganization Following a Stroke…….9

2. Objectives and Hypotheses……..17

3. Methods

3.1 Animals……18

3.2 Experimental Design……....18

3.3 TAM Administration……..…….……21

3.4 Surgical Procedures……...……..……21

3.5 String-Pull Task……..……..…22

3.6 Kinematic Assessment of String-Pull Motion Using DeepLabCuts……..…..……23

3.7 Perfusions and Sectioning……...…….27

3.8 Immunohistochemistry…….……27

3.9 Image Acquisition and Analysis……....……..……28

3.10 Stroke Volume Analysis……..…..…….……30

3.11 Animal Exclusion and Statistical Analysis…….……...…….…30

4. Results

4.1 String-Pull Behaviour……...……...….32

4.2 Sham and Stroke Mice have Similar Kinematic Movements During the String-Pull Task……...……...…35

4.3 Stroke Infarct Location and Volume……..……...43

4.4 Less Activated Cells are Labelled in the Ipsilesional M2 of Stroke Mice at the Pre-Stroke Baseline Compared to 2 dps……..……...……..……..45

4.5 No Difference in Active or Reactivated Cells at 2 dps Compared to 2 wps……..…..47

4.6 No Difference in Active or Reactivated Cells at the Pre-Stroke Compared to 2 wps……..……....49

4.7 Less Active Cells in Sham and Stroke Mice Express NeuN Following Surgeries.…51

5. Discussion

5.1 M2 Networks Remain Stable Throughout Stroke Recovery Despite Decreases in Active Cells at 2 dps…….53

5.2 Phenotype of Arc-TRAP and IHC Labelled Cells…….57

5.3 No Differences in Kinematic Performance Between Sham and Stroke Mice……..58

6. Conclusion……61

7. References…….……63

List of figures

Figure 1: TRAP transgenic mouse model….....11

Figure 2: Deficits are observed for mice performing the string-pull task acutely post-stroke.....13

Figure 3: String-pull behaviour in mice robustly increases cell activity in the motor cortex……16

Figure 4: Experimental timelines…….……..20

Figure 5: DLC analysis……..26

Figure 6: Stroke mice pull less string following photothrombotic stroke…….33

Figure 7: The distance travelled by the forepaws is not difference between stroke and sham mice……36

Figure 8: The movement speed of the forepaws is not different between stroke and sham mice……37

Figure 9: Stroke and sham mice have similar trends in movement scaling…….…..39

Figure 10: Sham and stroke mice have similar trends in path circuity movements…….....40

Figure 11: The bimanual coordination of sham and stroke mice are not different……..…..42

Figure 12: Photothrombotic strokes lesions……...…44

Figure 13: Decrease in active cells in the ipsilateral M2 cortex of stroke mice at 2 dps……...46

Figure 14: No differences in active or reactivated cells at 2 dps compared to 2 wps for sham and stroke mice……...……...……..48

Figure 15: No differences in active or reactivated cells before the stroke compared to 2 wps for sham and stroke mice…….…..50

Figure 16: Irrelevant of stroke injuries, less IEG+ cells are co-labelled with NeuN……...…..52

Supplemental Figure 1: Re-exposure is insufficient to increase the amount of string pulled overtime.…….…….62

List of abbreviations

ANOVA	Analysis of Variance
AP	Anterior-posterior
BSA	Bovine serum albumin
CIMT	Constraint-induced movement therapy
CreER	Cre-estrogen receptor recombinase
DAPI	Diamidodino-2-phenylindole
DMSO	Dimethyl sulfoxide
DLC	DeepLabCut
DPS	Days post-stroke
fMRI	Functional magnetic resonance imaging
FOV	Field of view
IEG	Immediate early gene
IHC	Immunohistochemistry
IP	Intraperitoneal injection
M1	Primary motor cortex
M2	Secondary motor cortex
MCAO	Middle cerebral artery occlusion
ML	Medial-lateral
MQ	Milli-Q
NaN3	Sodium azide
N.A.	Numerical aperture
NDS	Normal donkey serum

OH-TAM	4-hydroxytamoxifen
PBS	Phosphate-buffered saline
PET	Positron emission tomography
PFA	Paraformaldehyde
PRR	Proportional Recovery Rule
PT	Photothrombotic stroke
SEM	Standard error of the mean
SBR	Spontaneous biological recovery
tPA	Tissue plasminogen activator
TRAP	Targeted recombination in active populations
Tween-20	Polyoxyethylenesorbitan monolaurate
VSD	Voltage sensitive dye
WPS	Weeks post-stroke
YFP	Yellow fluorescent protein
2D	2-dimension
3D	3-dimension

Acknowledgements

I would first like to thank my family for all of their love, support and encouragement throughout all of my post-secondary studies. Without them, I would have never pursued my passion to study the brain and stroke recovery.

In addition, I would like to acknowledge all members (past and present) of the Lagace laboratory, as this project would not have been possible without their help. Thank you to Timal Kannangara, my first mentor in research, Marc Vani and Damian Chwastek who helped pilot the Arc-CreER^{T2}:Rosa-YFP$^{f/f}$ studies and to all my other lab colleagues, Yingben Xue, Alëna Kalina, Victoria Anne Purdy-Millaire, Maria Beryoza, Isabella Zabek and Maleeka Ellaithy, who have helped me tirelessly over the last years and have allowed me to achieve my academic endeavours. A special thanks to Gavin Heidenreich and Katie Neale for their support and guidance during the Deeplabcut setup and data analysis.

I would also like to thank my thesis advisory committee, Greg Silasi and Jean-Claude Béïque, for all of their academic and research related guidance.

Finally, I would like to take the time to thank my supervisor, Diane Lagace, for all of her help, guidance and support over the last seven years. I am beyond grateful that I was able to join your lab as a high-school graduate. Over the years, you have helped me gain confidence in my abilities, my spoken English and have helped me grown as a researcher and a person. Thank you for always being there to answer my questions and for being an amazing mentor.

1. Introduction

1.1 Stroke

A stroke occurs when a brain region is deprived of blood supply carrying oxygen and nutrients, leading to cellular death (AHA, 2022; Krueger et al., 2015). In 2019, strokes were the 2nd leading cause of death worldwide and were responsible for approximately 11% of total deaths according to the World Health Organization (WHO, 2020). Strokes have been further categorized as either hemorrhagic or ischemic based on how the blood supply is interrupted. Hemorrhagic strokes represent approximately 10% of all strokes and are caused by the rupture of one or multiple blood vessels causing excessive bleeding. Unfortunately, these injuries have a very high mortality rate of upwards of 50 % within the first year of the injury (Rymer, 2011). Ischemic strokes represent the remaining 90% of strokes and occur when cortical blood supply is interrupted as a result of clotted blood vessels. These strokes have a lower rate of morality but cause significant disabilities for more than 60% of stroke survivors (Kessner et al., 2019). Included within the types of ischemic injuries are transient ischemic attacks, or more often referred to as mini-strokes. Unlike ischemic strokes, these injuries only last for a few minutes and thus usually produce minimal neurological deficits, albeit, they do increase the risk for subsequent strokes by up to 40% (Johnston, 2002; Khare, 2016).

Due to recent increases in the awareness of early stroke symptoms (FAST: facial drooping, arm weakness, slurred speech), the development of *The Canadian Stroke Best Practice Recommendation,* and advancements in medical interventions for ischemic stroke, there has been an increase in the rate of survival after stroke (Lindsay et al., 2014). For example, acute stroke treatments includes the intravenous administration of tissue plasminogen activator (tPA) that was approved in 1996 (NINDS, 2022b). tPA is able to dissolves blood clots, restores blood flow and

thereby limits brain damage and resulting functional impairments (Cheng and Kim, 2015). In 2003, endovascular therapies consisting of the first endovascular thrombectomy device was also approved as a treatment for acute stroke (NINDS, 2022a; Smith et al., 2005). During these treatments, tubes are guided toward the occluded blood vessel, and the blood clot is removed through mechanical thrombolytics, either with stent-retrievers or aspiration catheters, which also restores blood flow and limits brain damage (Xing et al., 2020). Unfortunately, despite these new treatment options many do not have access to acute stroke treatments, either due to their lack of medical care access or the limited intervention window of the approved stroke treatments. Additionally, the growing rate of stroke survival has resulted in more stroke patients that are left with lifelong impairments. For example, in 2017, more than 400,000 Canadians were living chronic stroke-related disabilities (Heart&Stoke, 2017). Of these stroke patients, approximately 40% have moderate to severe deficits impeding their daily functions and requiring intensive rehabilitation and medical support (Heart&Stoke, 2017; Krueger et al., 2015). It is even more alarming that in the next 20 years, the number of patients living with strokes in Canada is predicted to double, which will induce a significant burden to stroke survivors, their families, and our health-care system.

For patients with chronic stroke disabilities, rehabilitation therapies are strongly recommended (Billinger et al., 2014; Langhorne et al., 2011). Given that the extent of stroke deficits varies for each patient, stroke rehabilitation therapies are administered in many forms which are often personalized to patients in order to meet their individual recovery goals (Pascual et al., 2018). Conventional motor rehabilitation interventions commonly include components of physical exercise and muscle strengthening (Langhorne et al., 2011). Constraint-induced movement therapy (CIMT) is one intervention that can be administered to patients within a few

months of their injuries (Kwakkel et al., 2015). CIMT consists of limiting the use the unaffected limb, thus, greatly increasing the used of the stroke affected limb of patients during their daily activities (Fleet et al., 2014). More recently, rehabilitation using virtual reality is being used and patients are showing some benefits in their motor and cognitive abilities post-stroke (Cortes-Perez et al., 2020; Rogers et al., 2019).

1.2 Spontaneous Biological Recovery Following Stroke

In the absence of any treatment following a stroke, it is remarkable that stroke survivors demonstrate innate improvements in motor function (Bernhardt et al., 2017; Grefkes and Fink, 2020). This recovery is referred to as spontaneous biological recovery (SBR) since it occurs in the absence of any treatment. SBR often leads to incomplete recovery of function in patients and only occurs within a critical time period following strokes. In humans, SBR can occur as early as a few days following the initial injury and last up to 3 months, at which time functional improvements slowly plateau (Bernhardt et al., 2017). In preclinical model, SBR can occur within hours of a cortical injury and last upward of a month, albeit, this recovery is dependent on the stroke location and size (Karthikeyan et al., 2019).

The extent of recovery in patients has been debated for over the last decade. This debate was started when Prabhakaran et al. (2008) used clinical predictors to model the degree of post-stroke recovery, and created the Proportional Recovery Rule (PRR). Within 3 to 6 months after a stroke, the PPR predicts that most patients with intact spinal cords and mild to moderate upper limb deficits, will recover approximately 70% of their initial stroke impairments (Kundert et al., 2019; Prabhakaran et al., 2008). Patients with severe impairments and unpreserved cortical spinal tract function are not subjected to this degree of recovery. Since then, multiple clinical and pre-clinical studies have validated the PRR in both the upper and lower limbs (Coupar et al., 2012;

Jeffers et al., 2018; Smith et al., 2017). However, contradicting findings have been reported and suggest that the proportional recovery model is not valid (Hope et al., 2019; Lee et al., 2021). Recent studies have suggested that there is bias in the evaluation of recovery in the PRR theory, which may contribute to inflate the effect size (Bowman et al., 2021; van der Vliet et al., 2020). Although the extent of recovery of stroke patients remains unknown, there is a general consensus that some degree of motor recovery does occur following strokes (Bernhardt et al., 2017; Langhorne et al., 2011).

Research has been focused on characterizing the mechanisms mediating SBR in order to harness its mechanisms to further improve stroke recovery. SBR is hypothesized to be accomplished through the upregulation of several forms of cellular plasticity in the adult brain, which includes mechanisms such as the production of adult generated neurones, angiogenesis and cortical reorganization (Ergul et al., 2012; Jones and Adkins, 2015; Williamson et al., 2019).

1.3 Cortical Reorganization in Humans

Cortical reorganization consists of the reallocation of function from the site of injury to surrounding and surviving brain regions (Grefkes and Ward, 2014). These brain regions can include the peri-infarct, or more distal sites within the uninjured contralesional hemisphere, the pre-motor cortex and the spinal cord (Binder et al., 2021; Brown et al., 2007; Grefkes and Ward, 2014; Johansen-Berg et al., 2002; Takatsuru et al., 2009; Wahl et al., 2014). In humans, functional neuroimaging is used as a non-invasive approach to study cortical reorganization. Positron emission tomography (PET) scan and functional magnetic resonance imaging (fMRI) have been used to map the changes in activity. Weiller et al. (1992) were one of the first to use PET imaging to show that regional cerebral blood flow increases in both the contra- and ipislesional sensorimotor cortex while patients utilized their affected hand more than 3 months following the

injury. Other studies who have investigated brain activity at a single time point have confirmed that bilateral activation patterns are observed post-stroke and have revealed that the increased activation of the contralesional primary motor cortex (M1), bilateral ventral premotor cortex and supplementary motor areas were common amongst stroke patients compared to healthy individuals (Rehme et al., 2012).

Longitudinal neuroimaging analysis of the motor maps of stroke patients have demonstrated that activation patterns change throughout stroke recovery. Tombari et al. (2004) have evaluated the changes in activity of the sensorimotor cortex following subcortical strokes. Within the first 20 days of the injury, hyperactivity of the contralesional hemisphere was observed and shifted to the ipsilesional sensorimotor cortex by 4 months post-stroke. Furthermore, Rehme and colleagues (2011) reported that the increase activity of the contralesional hemisphere did not occur immediately following stroke, but rather began approximately 5 days post-stroke, a critical time period during which motor recovery occurs. However, by 4-month, motor activation was limited to the injured cortex. These findings indicate that the increase excitatory neural activity is a time-dependent phenomenon and that early contralesional and chronic ipsilesional activation may play a supportive role in stroke recovery. Other studies have validated that lateralized activation restricted to the ipsilesional motor cortex in chronic stroke patients is associated with good motor recovery (Ward et al., 2003). Despite these findings, the role the contralesional hemipshere remains debated as chronic activation of the contralesional hemisphere has been observed in patients with good motor recovery post-stroke (Bütefisch et al., 2005).

Changes in functional connectivity (FC), the statistical relationship describing how the activity of brain regions covaries overtime, have also been assessed using fMRI to measure remapping. A cross sectional study on the FC of acute phase (4-7 days post-injury) stroke patients

reported that patients with different severities of somatosensory impairments, as measured by the Erasmus MC modifications to the Nottingham Sensory Assessment tool, had differences in somatosensory network connectivity (De Bruyn et al., 2018). Patients demonstrating more severe somatosensory impairments had significantly less interhemispheric and ipsilesional intrahemispheric FC compared to less impaired patients. Furthermore, brain regions with more structural and functional connections with the lesion site were subjected to a more extensive remapping overtime (Olafson et al., 2021). Individuals with greater stroke impairments also demonstrated greater functional reorganization which related to motor recovery by 6 months post-stroke.

Altogether, literature on human cortical reorganization post-stroke suggests that the bilateral activation patterns of early stroke patients are rescued overtime and restricted to the ipsilesional motor cortex. However, the roles of the contralesional hemisphere in stroke recovery remains debated. In addition, these studies demonstrate that both inter- and intra-hemispheric connections are altered with stroke severity and that brain regions with strong connections with the peri-infarcted cortex are subjected to more remapping overtime.

1.4 Cortical Reorganization in Preclinical Models

Preclinical studies have also examined the changes in cortical excitability of sensorimotor maps in the motor cortex that occur following strokes. The motor cortex is comprised the primary (M1) and secondary motor (M2) cortices that are responsible for the execution of motor function (Jeong et al., 2016). Similar to the clinical literature, preclinical studies focused on cortical reorganization have mostly assessed the M1 given its central role in the execution of motor function (Brecht et al., 2004). Cortical excitability has been assessed in behaving rodent models using genetically encoded Ca^{2+} indicators and voltage sensitive dyes to allow for *in vivo* imaging

(Brown et al., 2009; Lim et al., 2014). These studies have reported that stroke injuries can rapidly cause changes in excitability and reorganization in the ipsilesional hemisphere. Specifically, following mini-strokes, Mohajerani et al. (2011) observed a decrease in the activity of the ipsilesional hemisphere of stroke mice that occurred within 30 minutes of the injury. Sigler and colleagues (2009) also reported that sensorimotor maps can be altered within a few hours of a stroke and be rapidly redistributed, from the forelimb to hindlimb and posterior lateral sensory areas. Given that this redistribution of function occurred within hours, it can likely involve pre-existing surviving accessory pathways. Furthermore, in some studies the decrease in ipsilesional activity was reported to last upward of 1 week following a targeted photothrombotic stroke to the forelimb sensorimotor cortex (Brown et al., 2009; Lim et al., 2014). The decrease in ipsislesional activity was rescued overtime by the emergence of reorganized motor networks. Following forelimb-evoked depolarizations at 8 weeks post-stroke, activity began in the intact peri-infarcted cortex and spread horizontally to surrounding motor and hindlimb sensorimotor regions and also involved distant sites in the posteromedial retrosplenial cortex. Reorganization was also accompanied by high dendritic turnover, indicating the used of new structural circuits in the reorganized post-stroke brain (Brown et al., 2009). Furthermore, Lim et al. (2014) reported that sites with strong connections near the peri-infarcted cortex are more severely affected by the injury and tend to have less relative stroke recovery in comparison to regions with weaker connections to the stroke, thus suggesting that recovery in the peri-infarct is heterogenous.

The reduction in ipsilesional activity is also accompanied by increases in the activity of the contralesional hemisphere (Jones and Adkins, 2015; Mohajerani et al., 2011). The functional role of this increase in activity is however debated. Using muscimol to inactivate the contralesional hemisphere within hours of a stroke, Mansoori et al. (2014) reported that the early activation of

the contralesional hemisphere was detrimental to motor recovery post-stroke, as demonstrated by an increase in the motor performance of the paretic limb of rats within 2 months of the stroke injury. In contrast, others have suggested that the activation of the contralesionsal hemisphere may be neuroprotective (Biernaskie et al., 2005; Nishimura et al., 2007). For example, inhibition of the contralesional hemisphere of stroke injured rats using lidocaine impaired motor function of the stroke injured limb (Biernaskie et al., 2005). Furthermore, these preclinical findings align with clinical findings that have supported both beneficial and detrimental effects of contralesional activation during stroke recovery (Bütefisch et al., 2005; Ward et al., 2003).

Harrison et al. (2013) also added to the understanding of reorganization post-stroke by assessing the changes in sensory-motor map structures following stroke in sensory and motor areas. Displacement of maps differed with photothrombotic (PT) stroke of the same size within different locations. Motor strokes elicited new and more diffuse motor maps which maintained its position in motor regions, while sensory strokes induced a larger displacement of the sensory maps towards the motor forelimb areas. Consequently, this study suggests that stroke location mediates different cortical reorganization outcomes.

In contrast to studies suggesting that cortical reorganization occurs following a stroke, new evidence from Zeiger et al. (2021) argues against cortical remapping in the barrel cortex following a stroke. Zeiger and colleagues used an inducible TRAP (targeted recombination in active population) mouse model and reported that there was no cortical remapping following PT strokes targeted to the C1 barrel cortex. These findings were robustly confirmed through the use of intrinsic signal imaging and two-photo calcium imaging of sensory-evoked responses, where they reported no increases in the number of C1 whisker responsive cells within the adjacent D3 barrel region up to 1 month after the stroke. However, forced used therapy, accomplished by removing

all but C1 whiskers, increased the reliability of sensory-dependent responses from the remaining C1 whisker neurons in the peri-infarcted cortex. Based on previous findings in the sensorimotor cortex (Brown et al., 2009; Lim et al., 2014), the lack of reorganization reported in this study may be due to the cortical region investigated. Thus, it remains to be tested whether TRAP models would detect motor reorganization following a stroke localized within the motor cortex.

Altogether, the majority of the studies support the presence of reorganization following stroke, however the changes in the activity of motor networks that occurs during reorganization appears heterogenous, with all brain regions not subjected to the same extent of cortical remapping. This stresses the need to assess if and how cortical remapping occurs within all sensory and motor cortices following strokes of different sizes and locations.

1.5. Using a TRAP Model to Detect Cortical Reorganization Following a Stroke

In order to address the changes in reorganization following a stroke, our laboratory tested the ability of TRAP transgenic mice to reliably label active cell networks within the motor cortex following forelimb specific tasks. Specifically, we used the Arc-CreER^{T2}:Rosa-YFP$^{f/f}$ (YFP: yellow fluorescent protein) mouse model. Similar to all TRAP models, the Arc-CreER^{T2}:Rosa-YFP$^{f/f}$ (Arc-TRAP) mouse permit the labelling of active cells at a first time point using Tamoxifen (TAM) dependent recombination (Figure 1A). At a secondary time point, perfused mice can be stained against immediate early genes (IEG), such as c-Fos, using immunohistochemistry (IHC). Previously, c-Fos has been used to label cells at a second time point, as opposed to Arc, for 2 main reasons. First, the arc protein is highly enriched and accumulates near activated synapses in the dendrites of neurons, while c-Fos is a nuclear antigen, rendering colocalization assays easier (Guzowski et al., 2001; Tom Curran et al., 1984). In addition, both Arc and c-Fos have similar kinetics and are most often expressed within the same cells (Farris et al., 2014; Vani, 2018).

Altogether, the Arc-TRAP model allows for 3 distinct populations of cells to be labelled; 1) cells active at the first time point (YFP+), 2) cells activated at second time point (c-Fos+) and 3) cells that are reactivated (YFP+/c-Fos+). This is achieved because TRAP models; 1) do not rely on structure specific driving promoters but rather IEGs and 2) that IEG expression is transient following behaviours (Figure 1B).

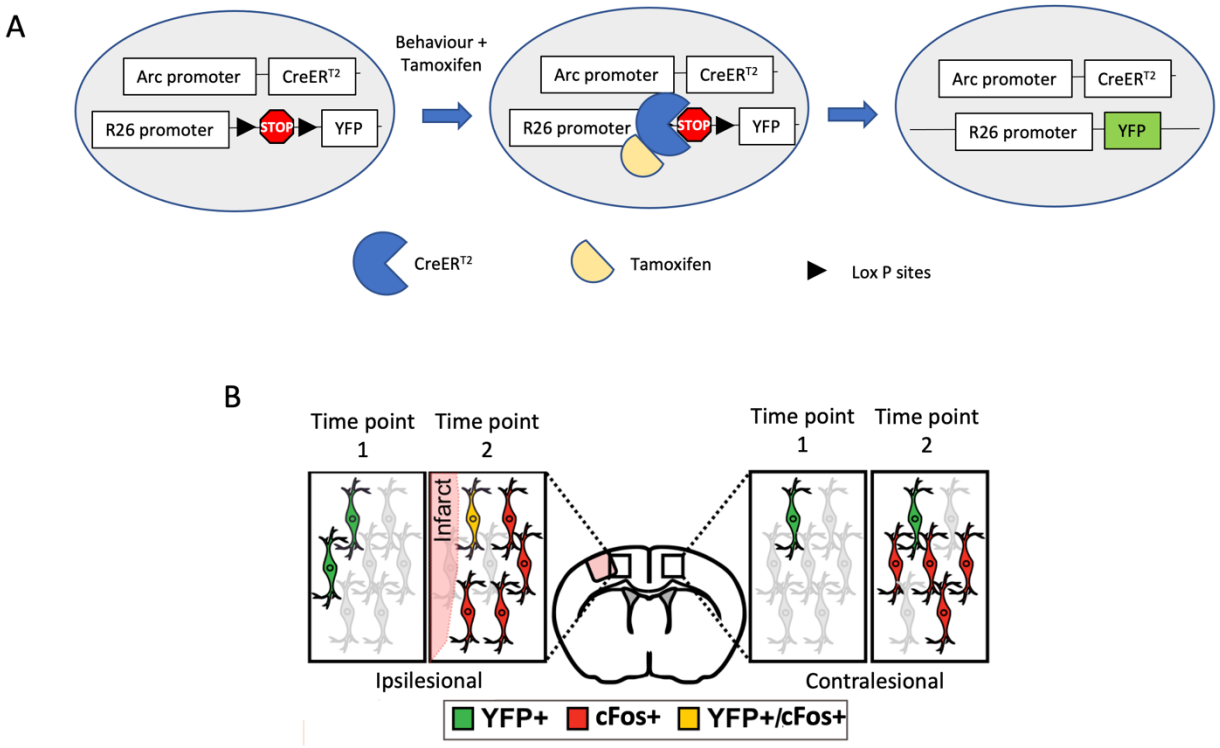

Figure 1: TRAP transgenic mouse model. (A) The immediate early gene, Arc, drives the expression of the Cre recombinase protein fused to a mutant form of the estrogen receptor (ER^{T2}). This protein complex is only responsive to exogenous tamoxifen. Once TAM binds its ligand, Cre is translocated to the nucleus where it excised floxed genes. In this model, a stop codon is removed, allowing for the permanent labelling of Arc positive cells at a behavioural time point. Through immunohistochemistry, active cells at a second time point can be labelled. (B) The TRAP model labels 3 distinct cell populations, either, cells active at time point 1 (YFP+), time point 2 (cFos+) and reactivated cells (YFP+cFos+).

The first studies performed in the Lagace laboratory using this model were done by Mark Vani, a previous Master student, and published in his thesis (Vani, 2018). Giving that the M2 is involved in motor learning, planning as well as the execution of motor tasks and that both M1 and M2 motor cortices shared similar projection areas in cortical and subcortical regions (Cao et al., 2015; Duan et al., 2021), these studies focused on examining reorganization in M2. This work used the Arc-CreERT2:Rosa-YFP$^{f/f}$ mice in conjunction with the rotarod behavioural task. The rotarod produced a robust activation of cells pre and 2 weeks post-stroke (wps) compared to home cage control mice, with approximately 65% of cells active at the first behavioural time point being reactivated after stroke. Despite these findings, no motor deficits were present following cortical injuries using this behavioural task. Since the rotarod task was not able to detect deficits in motor performance following stroke, an honors student, Damian Chwastek, followed-up on this study and assessed whether reorganization took place following a behavioural test capable of detecting stroke impairments (Chwastek, 2019). This work first assessed whether the bimanual string-pull task could detect deficits following a photothrombotic unilateral stroke injury. The rationale for using the string-pull task was based on previous work from Blackwell et al. (2018b), which reported the motor deficits of cortically injured rats using several outcome parameters. As shown in Figure 2A, the mice in the study performed the string-pull task prior to the stroke, at 2 day post-stroke (dps), 1 wps and 2 wps. At 2 dps, the mice pulled significant less string, which gradually returned to pre-stroke values by 1 wps (Figure 2B). In addition, although not statistically significant, another pilot study in this thesis demonstrated a 2-fold decrease in the amount of string pulled 2 dps, for stroke mice compared to sham surgery controls (Figure 2F). Overall, these studies suggested that the string-pull task could reliably detect reductions in the amount of string pulled, which is suggestive of motor impairments.

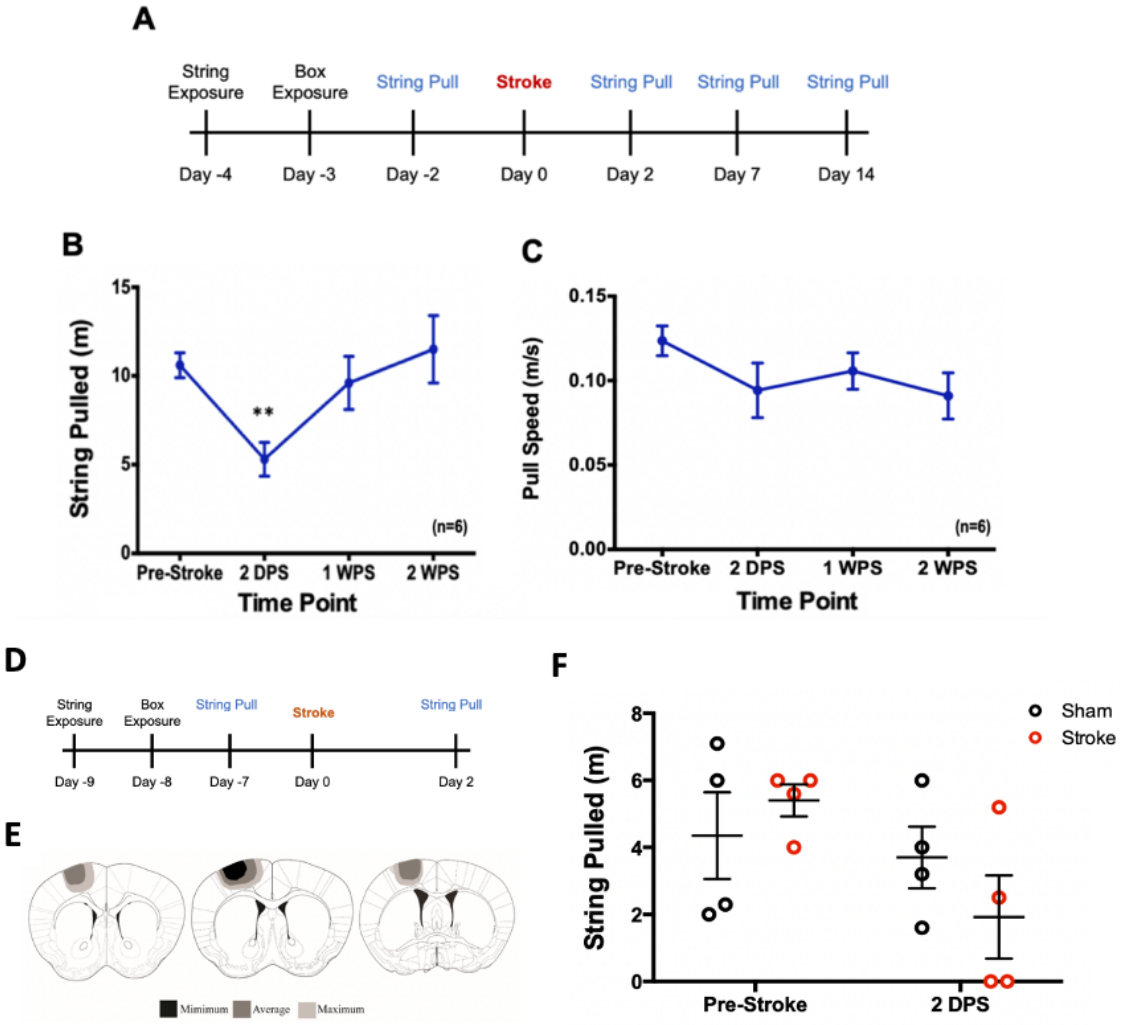

Figure 2: Deficits are observed for mice performing the string-pull task acutely post-stroke. (A) Behavioural timeline. Mice were trained on the string-pull task for 2 days (Day 1: string exposure and Day 2: box exposure). The string-pull task was performed 2 days prior to the stroke, at 2 dps, 1 wps and 2 wps. (B) Quantification of the amount of string pulled in metres. (C) Average rate at which the string is pulled (m/s). (D) Experimental timeline assessing the behavioural performance of sham and stroke mice. (E) Schematic representation of stroke location. (F) Amount of string pulled by sham and stroke mice before and after surgeries. Each dot on the graphs represents an individual animal. The means and SEM are also displayed on each graph (**, $p<0.01$). Figure modified from Chwastek (2019).

In addition to examining the amount of string pulled, these studies also showed that the speed at which the mice pulled the string remained the same before and after a stroke. Examination of the speed was performed by analyzing video recordings of the mice and examining the time when they started and stopped pulling the string divided by total string pulled (Figure 2C). One previous study has used markesless kinematic analyses to assess the string-pull behaviour of healthy mice and has examined the speed of the forepaws along with other outcome parameters, such as the distance of the hand movement as well as the efficiency of the string-pulling motion (Blackwell et al., 2018a). These kinematic outcome measures woud be interesting to use and assess the full spectrum of stroke deficits in mice, especially given previous work on rats which has used kinematics to assess the motor performance of rats on the string-pulling task after a cortical injury. Following the unilateral forelimb sensorimotor cortex devascularization of rats, Blackwell et al. (2018b) revealed a decrease in accuracy and the rhythmicity of movement between forepaws which was restored within a month. Thus, this study suggests that 2D kinematic analysis may accurately assess the stroke deficits of mice performing the string-pull task.

Damian also performed an experiment using the Arc-TRAP mouse model to examine the cells activated during the string-pull test compared to controls that did not perform the task. As shown in Figure 3, Arc-TRAP mice were randomly assigned to either perform the string-pulling task or were controls that completed a 15-minute trial within the string-pulling box without any string. Three hours following the behavioural task, mice were injected with the active form of TAM (4-OHTAM) to induce targeted recombination and permanently label active cells with YFP. 4-OHTAM was used to shorten the labelling period and assess short duration behaviours, as previously demonstrated (Guenthner et al., 2013). One week later, the string-pull and control mice underwent the same behavioural testing as baseline, and both groups were perfused following the

completion of the behaviour to assess the expression of c-Fos (Figure 3A). String-pull mice had no significant differences in the amount of string pulled at either time point (Figure 3B). The string-pull mice also had significantly more YFP+ and c-Fos+ cells in their motor cortex compared to the box controls (Figure 3C, 3D). Furthermore, there was a 3-fold increase in reactivated cells, as examined by the number of YFP+ and c-Fos+ cells, in the string-pull mice compared to the control mice (Figure 3F). These findings suggest that the string-pull task successfully increased motor cell activity in Arc-TRAP mice, and that the Arc-TRAP model is suitable to address changes in active cells involved during the performance of the string-pull task following stroke.

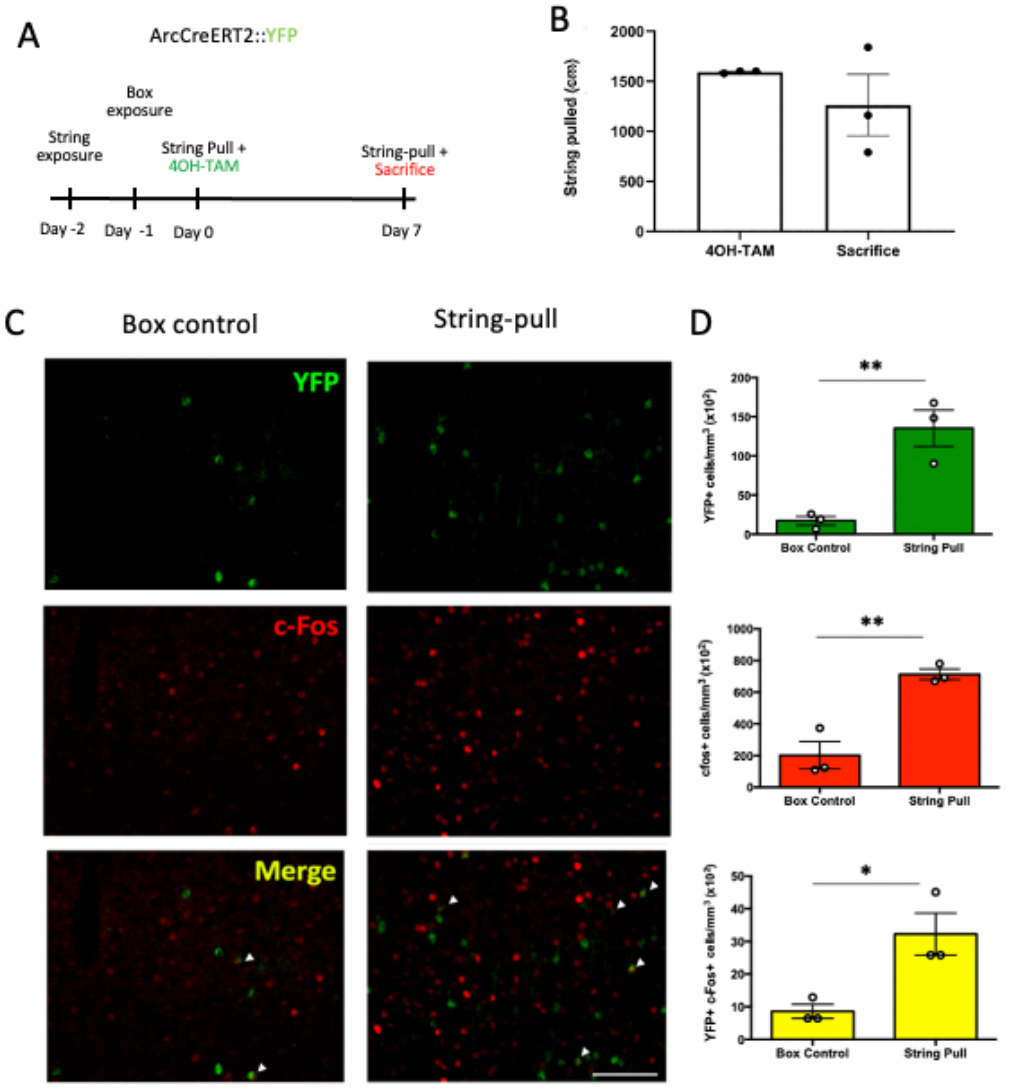

Figure 3: String-pull behaviour in mice robustly increases cell activity in the motor cortex. (A) Experimental timeline showing behavioural time points of control (mice were placed in the string-pulling box with no string; n=3) and string pull mice (n=3). (B) Amount of string pulled at baseline (day 0) compared to the experimental endpoint (day 7). (C) Representative images in the M2 cortex of the box control and string-pull mice, examining the active YFP+ cells (day 0); c-Fos+ cells (7 days) and reactivated cells (YFP+ and c-Fos+). (D) Quantification of active and reactivated cells. Each dot represents a single mouse. The means and SEM are displayed on each graph (*, $p<0.05$; **, $p<0.01$). Figure obtained from Chwastek (2019).

2. Objectives and Hypotheses

Objectives

This thesis work had the objectives to:

1. Identify what cells are recruited during the performance of the bimanual string-pulling task after stroke, as well as during stroke recovery using the Arc-CreERT2:Rosa-YFP$^{f/f}$ mouse model.
2. Perform kinematic analysis of the string-pull behaviour of mice to determine if there are differences in motor movements used following a stroke.

Hypotheses

1. Given the previous literature on reorganization in the sensorimotor cortex, we hypothesized that there would be less active and reactivated cells at 2 dps. In contrast, by 2 wps the decrease in active and reactivated cells would be rescued.
2. We also hypothesized that stroke mice would employ movements indicative of motor impairments on the string-pulling task, as measured by using DeepLabCut (DLC), such as acute decreases in movement rhythmicity post-stroke.

3. Methods

3.1 Animals

All animal procedures were approved by the University of Ottawa Animal Care Committee and were performed in alignment with the guidelines of the Canadian Council on Animal Care. Arc-CreER^{T2}:Rosa-YFP$^{f/f}$ mice of a C57/B6 background were obtained from Dr. Christine Denny's laboratory (Denny et al., 2014) and bred in-house at the University of Ottawa. The breeders were used to create male and female experimental mice that were heterozygous for Arc-CreER^{T2} and heterozygous for Rosa-YFP$^{f/f}$ (Arc-CreER$^{T2+/-}$:Rosa-YFP$^{+/-}$). All mice had *ad libitum* access to food as well as water and were housed in ventilated cages subjected to a 12:12 hour light/dark cycle in rooms in which the temperature and humidity were maintained at 23°C and 30-40%, respectively. Tail samples were collected at weaning of the mice and the extracts were genotyped as previously published (Denny et al., 2014; Lagace et al., 2007). At 10-12 weeks of age, the experimental mice were single housed 1 week prior to behavioural testing. A total of 74 Arc-TRAP mice were included in this study.

3.2 Experimental Design

A total of 60 Arc-TRAP mice (28 sham, 32 strokes) were utilized to complete 3 distinct behavioural study designs, as shown in Figure 4. Active and reactivated cells were quantified at either: 1) the pre-stroke baseline and 2 dps (Figure 4A, n=26 mice, completed in 2 cohorts), 2) 2 dps and 2 wps (Figure 4B, n=24 mice, completed in 2 cohorts), as well as the pre-stroke baseline and 2 wps (Figure 4C, n=10 mice, completed in 1 cohort). In all of the experimental designs, mice were first trained on the string-pull behavioural task. Mice were separated into two experimental groups: 1) sham control mice that received a sham surgery with no stroke (sham n=28) and stroke mice (n=32) which received a photothrombotic unilateral cortical stroke in their sensorimotor

cortex. The first active population of cells were labelled by administering OH-TAM to mice 3 hours following the performance of the string-pull task either before or after stroke and sham surgeries. At the second time point, mice were perfused 90 minutes following the string-pull behavioural task in order to detect c-Fos expression in the active cells. Only mice that pulled string at all time points were included in the study.

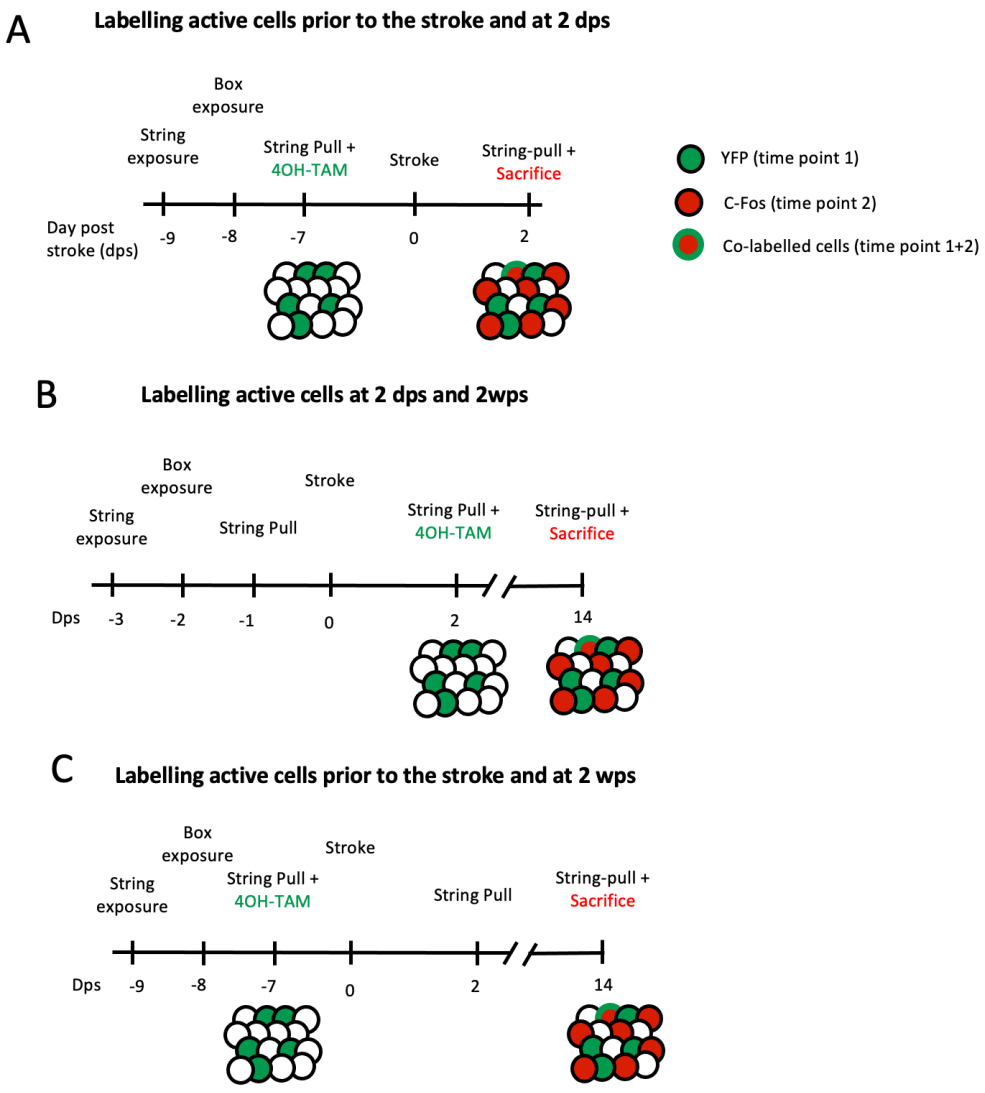

Figure 4: Experimental timelines. The Arc-TRAP transgenic mouse model was used to label active cells at a first time point after the performance of the string-pull task. Thus, active cells were permanently labelled with YFP. At a second time point, active cells were labelled with c-Fos. Reactivated cells express both YFP and c-Fos. Experimental designs used to assess active cells (A) before the stroke and at 2 dps, (B) at 2 dps and 2 wps as well as (C) prior to the stroke and at 2 wps.

3.3 TAM Administration

To label active cells at the first behavioural time point, mice receive an intraperitoneal injection (IP) of 4-OHTAM 3 hours following the behavioural task. A modified protocol from Ye et al. (2016) was used to prepare the 4-OHTAM solution which included 2% polyoxyethylenesorbitan monolaurate (Tween-20, P9416; Sigma) combined with 0.9% sterile saline added to 2.5 mg/mL 4-OHTAM (H6278; Sigma) dissolved in 5% dimethyl sulfoxide (DMSO, D5879; Sigma). Each mouse received 40 mg/kg of 4-OHTAM. Mice remained in the behavioural room (with normal light cycle) until the following morning to minimize background labelling of active cells.

3.4 Surgical Procedures

The photothrombotic stroke model was used to induce a unilateral ischemic stroke within the sensorimotor cortex of mice, as previous described in other studies (Kannangara et al., 2018; Zeiger et al., 2021). Mice were first placed underneath a heat lamp while being anesthetized using 5% isoflurane delivered with flowing oxygen (~1.5L/minute). To prevent dehydration, the mice received a subcutaneous injection of saline (~0.5mL). The mice were then transferred to a stereotaxic apparatus and placed on feedback heat pad with rectal probe in order to maintain their body temperature to approximately 37±1°C. For the rest of the surgical procedure, the delivered isoflurane was reduced to approximately 2 %. Rose Bengal (10 mg/ml, Sigma, diluted in 1x phosphate-buffered saline (PBS)) was administered through an IP injection. During the next 5 minutes, a small incision was made to expose the skull and bregma. A green laser (~20 mW, 532 nm, Beta Instruments) was aligned with the stroke coordinates measured in relation to bregma (0.7 mm AP, 1.5 mm ML and 2.5 cm laser height). The laser was then turned on 5 minutes after the incision was made and was left on for a period of 10 minutes to photoactivate the dye and induce

a stroke within the sensorimotor cortex. After the irradiation, the incision was closed using vetbond glue and topical 2% bupivacaine was applied over the incision site. Sham control mice received a similar surgery, with the exception that the laser was not turned on.

3.5 String-Pull Task

The bimanual string-pull task protocol was modified from previous protocols published by the Wallace group (Blackwell et al., 2018a; Blackwell and Wallace, 2020; Blackwell et al., 2018b). Prior to starting the sting-pull test, mice were handled once per day for 3 consecutive days as a form of habituation to the experimenter. For the following 3 days, IP injections (200 ml of saline) were administered on altering sides of the body to reduce stress associated with IP injections. The mice were then left for a single day in their home cage prior to beginning the string-pulling task training. The two days of training consisted of:

Training Day 1) Mice were placed in the behavioural room to habituate for a minimum of 30 minutes. Mice were then individually placed in an empty mouse housing cage and exposed to 15 strings (5x30cm, 5x60cm, 5x100cm; string is 100% cotton, 0.2 cm in diameter) for 1 hour. The number of strings pulled was noted.

Training Day 2) Mice were left to habituate in the behavioural suite for a minimum of 30 minutes. Mice were individually placed in a clear unbaited (no string) string-pulling box (13.3 cm x 7.5 c, x 26 cm) for 20 minutes as a form of habituation to the box in order to reduce anxiety, as well as allow for explorative behaviour that could also produce cell activation during the performance of the task.

On the following day, mice performed the string-pulling test after 30 minutes of habituation. Mice were placed in the string-pulling box for 15 minutes with 2 metres of cotton string. Once the entirety of the string was pulled, the box was baited with another string until the

end of the 15-minute trial. The experimenter remained in the behavioural testing room throughout the trials. The total amount of string pulled was measured for each animal. An Ethovision camera placed above the behaving mice also recorded the string-pull task. In addition, post-stroke mice performed the same string-pull behavioural task, with the exception of the pre-stroke training protocol.

3.6 Kinematic Assessment of the String-Pull Motion Using DeepLabCuts (DLC)

The 2D kinematic assessment of the string-pull behaviour was performed prior to the stroke, at 2 dps and 2 wps. The workflow for the kinematic assessment is shown in Figure 5. As depicted in Figure 5A, a high-speed FLIR camera was placed in front of the string-pulling box to record the behaving mice. The entire mouse was visible in the camera's field of view. To increase the efficiency and accuracy of DLC to label the forepaws of mice, an infrared light source was placed beside the camera while the lights in the room were set to approximately 80 lux. A solid plastic separator was placed between the behaving mice and the experimenter. Every time the mice approached the string and began to pull, the experimenter began recording the event using the SpinView camera software. The software settings used included recordings of 120 frames per second, an exposure time of 5000 μm and a digital gain manually set to 12 db. The aperture on the FLIR camera was also completely opened.

For the analysis of the videos, iPython was used to launch DLC and its graphical user interface. Multiple networks including, ResNet-50, EfficientNet and MobileNet were tested to determine which network was better fitted for the dataset based on the lowest pixel errors between the automated and manually labelled frames. We found that ResNet-50 was the most accurate network (data not shown), which is in alignment with a review from Mathis et al. (2020), that also noted that ResNet-50 is one of the most commonly used networks for DLC analysis.

To first train the ResNet-50 neural network, approximately 80 frames from video recordings of 2 animals at the Pre, 2 dps and 2 wps time points were used. Labels were manually placed overtop the left and right forepaws (Figure 5B). Active learning was then used to refine mislabeled frames and retrain the network accordingly. In total, 6 training iterations were conducted. This entailed manually refining the mislabelled frames after each iteration until a low pixel labelling error was achieved. Approximately 150 aberrantly labelled frames were manually labelled throughout all iterations. For each x and y forepaw coordinate, likelihood measures were generated. A threshold value of 0.1 was used to remove some of the remaining mislabeled frames (~ 5%), as previously published (Mathis et al., 2018; Nath et al., 2019). These values were excluded from all future kinematic analyses.

An R script was then used to analyze all csv. files obtained from the DLC analyses that was created by Katie Neale in Dr. Silasi's laboratory. Within this script, the 2D movement of the forepaws of were tracked through bouts of string-pulling activity and further separated into 2 phases, the reach and withdraw phases (Figure 5C-D). The reach phase was defined as upward movements from the bottom to the top of the field of view, while the withdraw phase was defined by downward movements from the top to the bottom of the field of view. From the tracked 2D movement of the forepaws, the distance, the speed, the movement scaling, the path circuity and the bimanual coordination were measured for each forepaw. The Euclidian distance was measured as the shortest distance between the beginning and the end of a phase. The speed was calculated using the frame rate and the number of frames used to travel each reach and withdraw phases. The movement scaling was calculated as the correlation between the Euclidean distance and the peak speed. The path circuity was defined as the ratio of the Euclidean distance and the total travelled distance. More direct paths of motions approach a ratio value of 1, while more complex movements

are closer to 0. The bimanual coordination was measured as the correlation between the distance travelled by the forepaws. A perfect negative correlation describes forepaws travelling in opposite phases of movements while forepaws that are positively correlated are travelling within the same phase. Mice with poor video quality (e.g. mice that did not face the camera while pulling) resulting in aberrantly labelled frames (n=5 at 2 dps) or mice that did not pull any string were excluded from the kinematic analysis (n=11 at the post-stroke time points).

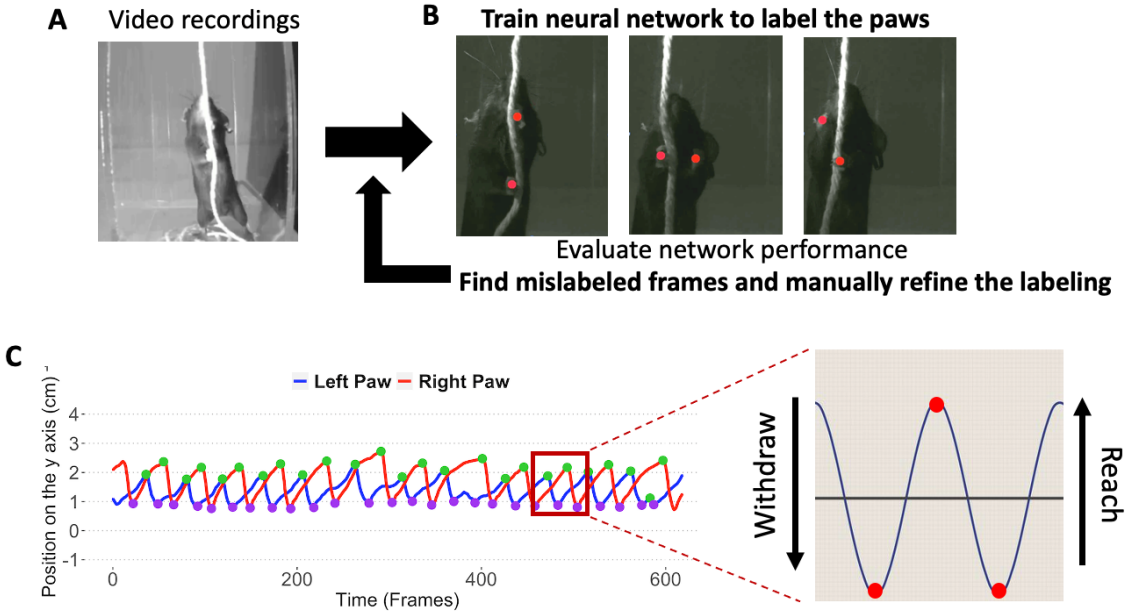

Figure 5: DLC analysis. (A) Representative single frame of a mouse performing the string-pull task. (B) Training of the DLC ResNet50 neural network. Labels are placed on the right and left forepaws to track forelimb movement. Mislabeled frames are manually refined to increase the labelling efficiency of the network. The trained network is then used to obtain the 2D coordinates of the forepaws in each frame. (C) Representative tracked movement of the left and right forepaws of behaving mice. Tracked movements are further separated into reach (upward movement) and withdraw (downward movement) phases.

3.7 Perfusions and Sectioning

All mice were anesthetized with IP injections of Euthanyl (~0.07ul/mouse) 90 minutes following the string-pull task in a room adjacent to the behavioural testing room. Mice were transcardially perfused with cold PBS and 4% paraformaldehyde (PFA) diluted in PBS. Brains were carefully removed, postfixed in a solution of 4% PFA in 1xPBS for 1 hour and cryoprotected in 30% sucrose and 0.1% sodium azide (NaN_3) in PBS (4°C). Using the freezing Leica SM 200 R sliding microtome (Leica Microsystems), 35 μm coronal sections between the olfactory bulb and the hippocampus were cut and stored in 0.1% NaN_3 in 1xPBS at 4°C.

3.8 Immunohistochemistry

All fluorescent labelling and quantification were done using free-floating immunohistochemical staining. A 2-day protocol was used to stain YFP+ and c-Fos+ cells. On day 1, the sections were washed in 1xPBS (3x 5 min) followed by washes in PBT solution (2x 5 min) freshly made containing 0.1% Triton-X, 0.1% bovine serum albumin (BSA) in 1xPBS at a pH of 7.4. After washing, the sections were incubated in a blocking solution (5% normal donkey serum (NDS), 1% BSA, 0.5% gelatine diluted in PBT) for 2 hours. All sections were then left overnight (12-24 hours) at 4°C on a shaker in the primary antibody solution that contained the blocking solution mixed with a 1:500 dilution of the chicken anti-GFP (GFP879484; Aves) and the rabbit anti-c-Fos (ab190289; Abcam) primary antibodies. On day 2 of the protocol, sections were washed with the PBT solution (5x 5 min) and then placed in the secondary antibody solution that contained a 1:500 dilution of AlexaFluor 488 anti-chicken (703-165-155, Jackson ImmunoResearch) and Cy3 anti-rabbit (711-545-152, Jackson ImunoResearch) antibodies, and left covered for 2 hours at room temperature on a shaker. Following the incubation in the secondary antibodies, the sections were washed in 1xPBS (3x 5 min) and then counterstained for 2.5 minutes

on the shaker using a 1:10000 dilution of DAPI (4′, 6-diamidine-2′- phenylindole dihydrochloride; 10236276001, Sigma) in 1xPBS. Sections were washed in 1xPBS (5 minutes at room temperature) prior to mounting onto Superfrost microscope slides. The slides were then coverslipped using Immunomount (2860060; Fisher) and stored at 4°C until imaging.

A free-floating IHC protocol was used to detect YFP, c-Fos and NeuN. Sections were washed in 1xPBS (3x 5 min) and incubated in a blocking solution made with 3% NDS in carrier solution (0.1% Triton X-100 & 0.1% Tween-20 in 1xPBS) for 1 hour. The carrier solution was used to make a 1:5000 dilution of the primary antibodies consisting of chicken anti-GFP (GFP879484; Aves), guinea pig anti-NeuN (3238431; MilliporeSigma) and rabbit anti-c-Fos (ab190289; Abcam)) antibodies. Sections were placed on a shaker overnight (12-24 hours) at 4°C. The following morning, sections were washed with 1xPBS (3x 5 min) prior to a 2-hour incubation in the secondary antibody solution including the carrier solution with a 1:500 dilution of Alexa Fluor 488 α-chicken (703-546-155; Jackson ImmunoResearch), CY5 α-rabbit (711-175-152; Jackson ImmunoResearch), and CY3 α-guinea pig (706-165-148; Jackson ImmunoResearch). Sections were washed in 1xPBS (3x 5 min), counterstained with DAPI for 5 minutes and finally washed in 1xPBS prior to mounting.

3.9 Image Acquisition and Analysis

All images were taking in the Cell Biology and Image Acquisition core at the University of Ottawa and analyzed using either Imaris or Zen imaging software. One fluorescent image per mouse was taken in matched coronal sections (~0.75 mm from bregma) and used to count the number of YFP+ and c-Fos+ cells. Three field of views (FOV) (447.63 μm x 335.40 μm) of the intact secondary motor cortex were imaged from both the ipsilesional and contralesional hemispheres within the same section. Z stacks were taken at 1 μm on the Zeiss Observer 1 (n=8

mice), or Zeiss Observer 7 microscope (n=66) with apotome. Similar cell counts were verified to be obtained from the Observer 1 and Observer 7 systems. Using either scope, the images were obtained using a 20x air immersion objective (N.A. = 0.8 plan-apochromat).

To determine if the YFP+ and c-Fos+ cells expressed NeuN, images were obtained from 6 mice (3 sham and 3 stroke) per timepoint. Z stacks were taken using the Zeiss Observer 7 microscope with the apotome using a 40x oil immersion objective (N.A. = 1.3 fluar) and 3 FOVs (332.80 µm x 332.80 µm) were taken in each hemisphere.

The Imaris imaging software was used to quantify the number YFP+, c-Fos+ and YFP+c-Fos+ cells. The diameter of YFP+ and c-Fos+ cells were first determined for each animal. These values were used to automate the labelling of all cells. We set a conservative labelling threshold and then manually confirmed the labelling for each FOV. All labelled cells expressed DAPI. To determine if cells were YFP+c-Fos+, the colocalization feature in Imaris was used and the radius of the largest average cell population (YFP) was set as the maximum cell radius. Manual quantification of the colabelled cells (~50/50 cells) matched the automated colocalization analyses during pilot studies.

The same quantification approach was used to determine the number of YFP+NeuN+, c-Fos+NeuN+ and YFP+c-Fos+NeuN+ cells, with the exception that grids of 100 µm x 100 µm (9 full squares/FOV (332.80 µm x 332.80 µm)) were superimposed on the images and only grids with YFP and c-Fos were quantified. Due to some technical issues with importing images into Imaris, 6/18 images were analyzed in Zen Blue software using the same protocol. In total, 3 sham and 3 stroke mice per experimental cohort (pre vs. 2 dps, 2 dps vs. 2 wps and pre vs. 2 wps) were used. Animals from 2 distinct behavioural cohorts were combined at each time point to increase the sample size (6 sham and 6 stroke mice per time point). At the pre-stroke and 2 wps time point,

YFP and c-Fos cells from 2 experiments were quantified respectively. At 2 dps, YFP from one animal cohort and c-Fos from another cohort of mice were quantified.

3.10 Stroke Volume Analysis

Stroke volumes were measured with cresyl violet for all mice who received a stroke, using our lab previously published methods (Kannangara et al., 2018). Briefly sections were sequentially dehydrated in 70% ethanol (10 dips), 95% ethanol (20 dips) and 100% ethanol (20 dips), then rehydrated in 95% ethanol (20 dips), 70% ethanol (10 dips) and milli-Q (MQ) water for 1 minute. The next step consisted of staining the brain sections for approximately 5-7 minutes with 0.25% cresyl violet dissolved in acetate buffer at a pH of 4 (0.5% sodium acetate, 0.003% acetic acid, 1.4% ethanol in MQ H_2O). Following the staining, slides were washed in MQ water (10 dips), 70% ethanol (10 dips) and 95% ethanol (10 dips). This was followed by 6-10 dips in 0.25% glacial acetic acid dissolved in 100% ethanol, 10 dips of 95% ethanol and 10 dips in 100% ethanol. Slides were then washed twice with the cleaning agent cirtrosolv (22-143-975; Fisher) for 1 and 3 minutes respectively. Finally, DPX mounting media (44581; Sigma) was used to coverslip the slides.

Infarct sizes were determined by imaging each section using the bright field Zeiss AxioScan slide scanning microscope at the Louise Pelletier Histology Core Facility. Infarct sizes were measured using the Zeiss Blue software. The infarct lesions were traced in each coronal sections to determine the area of the stroke lesions. Based on the thickness of the cut tissue (35μm), the overall volume of the lesion was determined.

3.11 Animal Exclusion and Statistical Analysis

All data in this study is presented as the mean ± standard error of the mean (SEM). Individual dots on the graphs represent a mouse and the bars represent the average for all the mice in the group. A total of 2 behavioural cohorts were done per experiment (Pre-2 dps and 2 dps-2

wps), with the exception that one cohort was included for the Pre-2 wps experiment. No effect of sex was present in sham or stroke mice, nor was there any difference between behavioural cohorts. Thus, all behavioural data was combined. Cell quantification was separated given differences in the number of active cells. In total, 17 mice were excluded from our analysis due to the lack of string-pulled (n=11), unsuccessful stroke lesions (n=1) and poor video quality for the kinematic analyses (n=5).

Two-tailed paired t-tests were used to assess differences between 2 groups (Figure 2, Figure 3 and Supplemental Figure 1). Given the absence of significant differences between behaviour cohorts, string-pull performances were combined from all 3 experimental study designs. For all the combined behavioural experiments (string pulled and kinematic performance), the performance of less mice was measured at 2 wps given that the experimental endpoint of some experiments was at 2 dps. As such, a mixed effect model was used instead of an ANOVA which cannot tolerate missing values for its analysis. Given there was significant differences in the cell counts between the different cohorts, results are shown and were analyzed for each experiment design separately using an ANOVA analysis. If there was a significant main effect, multiple comparisons were performed using the Bonferroni's and Sidak's post hoc analysis for the ANOVA and Mixed effect model, respectively. Significance was set at $p<0.05$ for all statistical tests.

4. Results

4.1 String-Pull Behaviour

After habituation to the string-pull task and prior to the surgeries, both sham and stroke mice pulled approximately 700-750 cm of string during a 15-minute behavioural trial (Figure 6A). Overall time and interaction effects were reported for both the amount of string pulled and the delta change analysis throughout the behavioural time points (Figure 6A-B). Following surgeries, both stroke and sham mice pulled significantly less string at 2 dps compared to the amount pulled before the stroke (Figure 6A). This was unexpected for sham mice, given Damian's pilot studies and the previously published stable performance of non-cortically injured rats on the string-pulling task, when measured over 2 months following brain injury (Blackwell et al., 2018b; Chwastek, 2019). In order to account for the individual variability in the performance of mice, as well as the difference in the amount of string pulled before and after surgeries, the delta change of the amount of string pulled was calculated. This analysis revealed that the stroke mice had an approximate and significant 2-fold reduction in the amount of string pulled at 2 dps compared to sham mice (Figure 6B). Additionally, examination of the amount of string pulled between 2 dps and 2 wps, by assessing either the total amount of string (Figure 6A) or the delta change (Figure 6B), revealed significant behavioural improvements with more string being pulled at 2 wps for the stroke mice, which is suggestive of SBR (Karthikeyan et al., 2019). However, the recovery was only partial, as the amount of pulled string at 2 wps did not return to the amount pulled at baseline (Figure 6A).

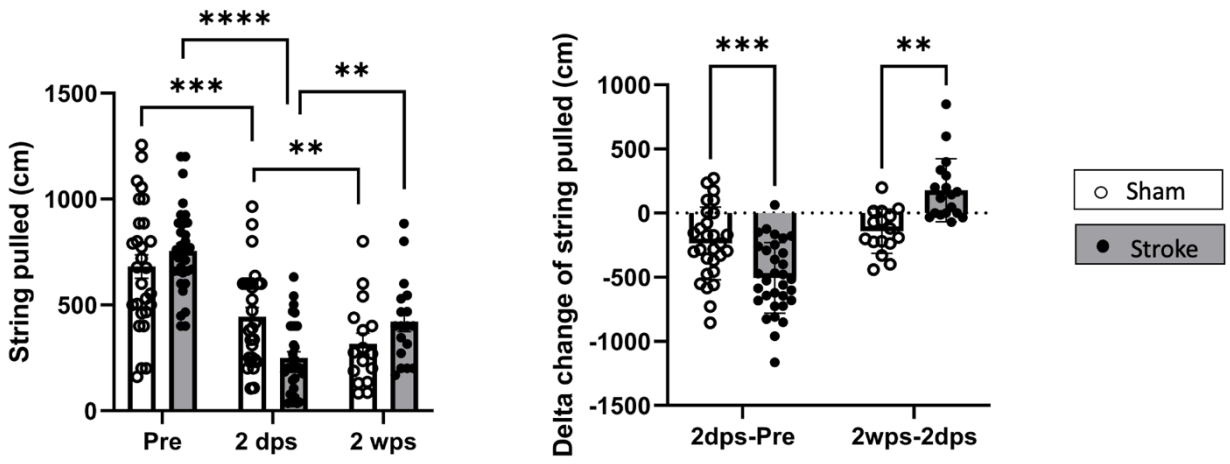

Figure 6: Stroke mice pull less string following photothrombotic stroke. (A) Amount of string pulled by the sham and stroke mice before surgery (pre), 2 dps and 2 wps (ANOVA: $F_{(time,1.7, 77.1)}$=76.1, p<0.0001, $F_{(interaction, 2, 90)}$ = 11.4, p<0.0001). (B) Delta change of the amount of string pulled comparing the stroke and sham mice at 2 dps minus pre, or 2 wps minus 2 dps ($F_{(time,1, 90)}$ = 49.4, p<0.0001, $F_{(interaction, 1, 90)}$ = 28.0, p<0.0001). Each dot on the graphs represents an individual animal (**, p<0.01; ***, p<0.001).

For the sham mice, it was also unexpected that the total amount of string pulled significantly decreased between Pre and 2 dps, as well as between 2 dps and 2 wps (Figure 6A). In order to try to understand the reduction in the sham mice behavioural performances, two pilot experiments with small sample sizes were performed, as shown in Supplementary Figure 1. To determine if a coincidental effect of surgery might account for the reduction in string pulled, a no surgical behavioural cohort was completed, where the mice remained in the home cage on the surgical day. This experiment demonstrated that the home cage mice also had a decrease in the amount of string pulled, and that the magnitude of this decrease in performance was similar to previous experimental sham cohorts (Supplementary Figure 1A compared to Figure 6). To determine if the reduction in sham performance was a result of mice forgetting how to perform the string-pull task after surgery, another experiment was performed where mice were re-expose to the string-pulling task. In this experiment, approximately 2 weeks following the sham control surgeries, mice were separated into 2 groups; 1) mice re-exposed to the string-pull task one day prior to testing and 2) mice that were not re-exposed. As shown in Supplementary Figure 1B, the total amount of string pulled by both groups was similar to the amount pulled acutely following sham surgeries (Figure 6), suggesting that re-exposure was insufficient to maintain behavioural performance at later time points and that mice do not appear to forget how to perform the task.

Altogether, the string-pull behavioural data indicates that both sham and stroke mice have reductions in the total amount of string pulled 2 days after sham or stroke surgery. However, analysis of the change in the amount of string pulled between the time points revealed that the stroke mice had a larger reduction in pulled string compared to sham mice, indicative of stroke-induce deficit, as well as a partial recovery in performance at 2 wps.

4.2 Sham and Stroke Mice Have Similar Kinematic Movements During the String-Pull Task

To assess the full spectrum of deficits and recovery, kinematic analyses of movement was also measured using DLC to analyse forepaw movements of the mice during the string-pulling task. Movements performed during the string-pull task were separated into reach and withdraw movements, as previously described by the Wallace group (Blackwell et al., 2018a; Blackwell and Wallace, 2020; Blackwell et al., 2018b). This analysis was done on 27 mice (13 shams and 14 stroke), from a total of 2 experiments (Pre Vs. 2 dps and 2 dps Vs. 2 wps).

As shown in Figure 7, at baseline the ipsilateral and contralateral forelimb of sham and stroke mice moved approximate 1.3 cm during the reach and withdraw phases. After stroke the total distance travelled by each forepaw was also similar between sham and stroke mice (Figure 7A-D). The delta change analysis also showed that the total travelled distance for each limb remained consistent overtime, as well as between sham and stroke mice (Figure 7E-H).

Similar findings were observed when measuring the speed of the reach and withdraw phases (Figure 8A-H). At all behavioural time points, the forepaws of both sham and stroke mice moved at ~5 cm/s during the reach phase, and ~10 cm/s during the withdrawal phases. It was unexpected to find that forepaw movements were faster during the withdraw phase given that Blackwell et al. (2018b) have previously reported no differences between movement phase speeds of control and cortically lesioned rats.

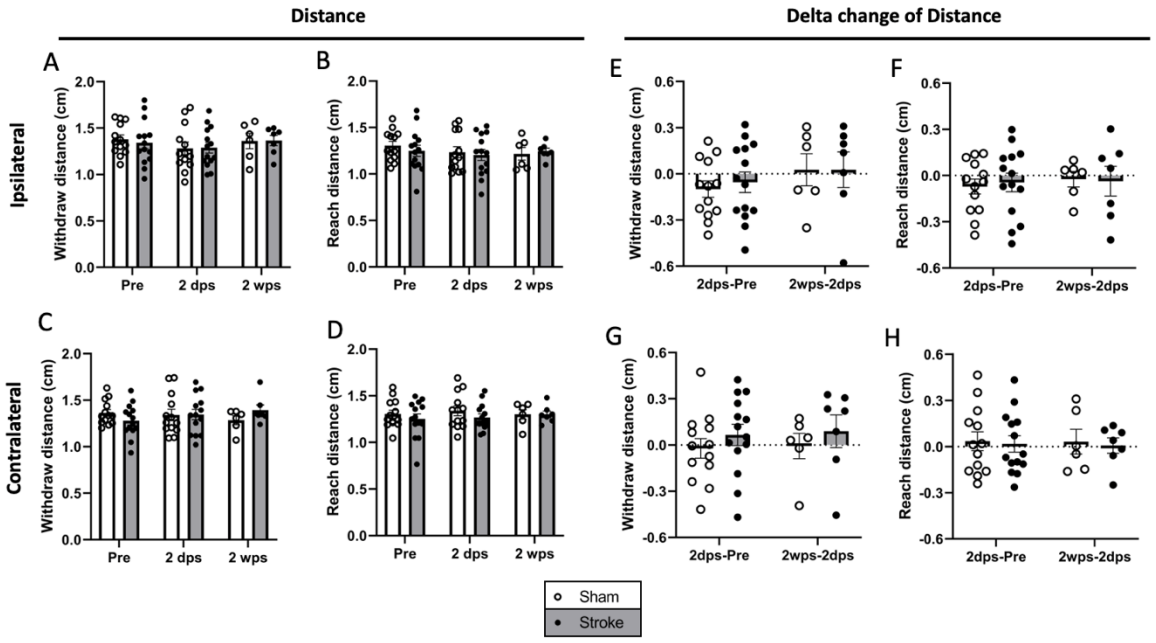

Figure 7: The distance travelled by the forepaws is not different between stroke and sham mice. Quantification of the distance travelled by the ipsilateral forepaw during the withdraw (A) and reach (B) phases of motion. Travelled withdraw (C) and reach (D) distance of the contralateral forepaw. Delta change analysis of the travelled distance (E-H) for each motion of the string-pull task. Each dot on the graphs represents an individual animal.

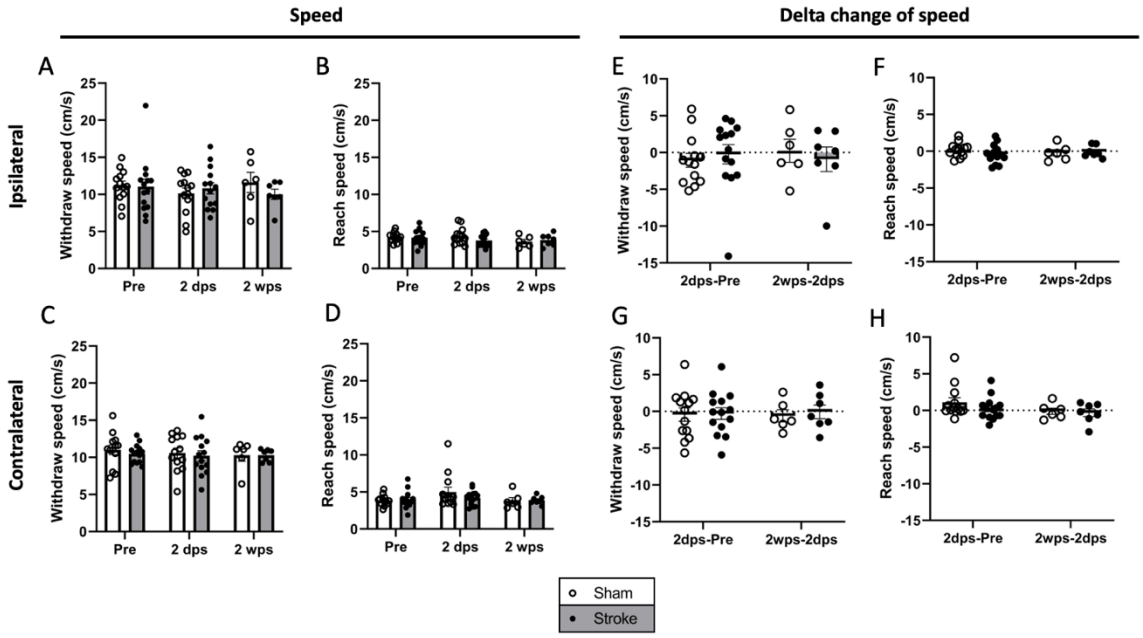

Figure 8: The movement speed of the forepaws is not different between stroke and sham mice. Quantification of the speed travelled by the ipsilateral forepaw during the withdraw (A) and reach (B) phases of motion. Travelled withdraw (C) and reach (D) speed of the contralateral forepaw. Delta change analysis of the travelled speed (E-H) for each motion of the string-pull task. Each dot on the graphs represents an individual animal.

Movement scaling was also measured by determining the correlation coefficient between the peak speed and Euclidian distance. The mean movement scaling score for all limbs and time points, in either the withdrawal or reach phase, and for either sham or stroke mice revealed a positive correlation between the speed of movement and the distance travelled (Figure 9A-D), as previously demonstrated in rats (Blackwell et al., 2018b). For the movement scaling of the reach and withdraw phases, no group or time differences were observed for both limbs (Figure 9A-D). For the DLC analysis, there was a significant overall difference between time points examined for the withdraw movement of the contralateral forepaw ($F_{(time,1,36)}$=7.4, p=0.01) (Figure 9E-H). Subsequent post-hoc analysis revealed a significant change in the movement scaling of sham mice from the pre-stroke baseline to 2 wps. However, a similar decrease in movement scaling was observed for both groups by 2 wps (Figure 9G).

To assess the complexity of the paths taken by the forepaws during string-pulling, the path circuity ratio consisting of the total distance travelled and the Euclidean distance was analyzed. At baseline, sham and stroke mice had similar and high path circuity ratios of approximately 0.7-0.8 (Figure 10A-D). The path circuity of in the ipsilateral forepaw during the withdraw and reach, as well as between sham and stroke mice remained consistent until 2 wps (Figure 10A-B). For the withdraw phase of the contralateral forepaw, there was also no differences in path circuity between time points, or between the sham or stroke mice (Figure 10C). In contrast, for the contralateral forepaw reach phase, there was an overall significant difference between time points ($F_{(time,1.4,25.0)}$ = 3.9, p=0.047) and significant decrease in sham performance at 2 dps (Figure 10D). Furthermore, when analyzed using delta change, both experimental groups showed similar trends with no significant differences observed for any limbs nor movement phases overtime, indicative of similarities in path circuity for both the sham and stroke mice (Figure 10E-H).

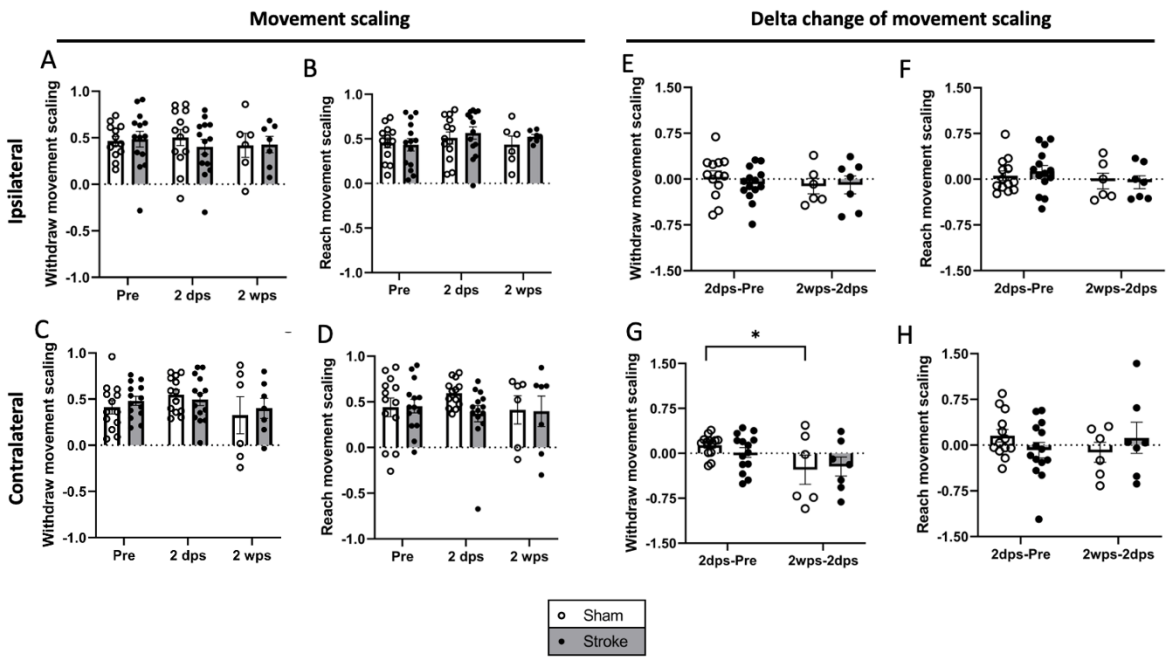

Figure 9: Stroke and sham mice have similar trends in movement scaling. Quantification of the movement scaling for the ipsilateral paw during the withdraw (A) and reach (B) phases of motion. The movement scaling for the contralateral forepaw during the withdraw (C) and reach (D) phases. Delta change of the movement scaling for the withdraw and reach phases of each forelimb (E-H) (*, $p<0.05$). Each dot on the graphs represents an individual animal.

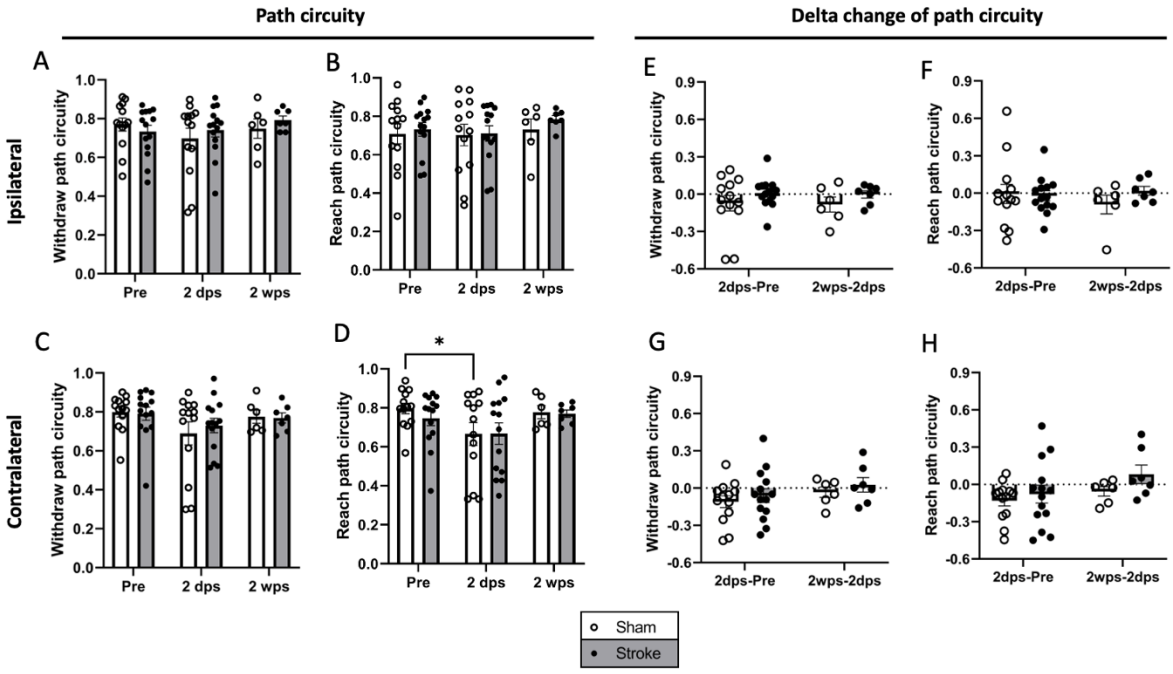

Figure 10: Sham and stroke mice have similar trends in path circuity movements. Quantification of the path circuity outcome parameter for the ipsilateral forepaw during the withdraw (A) and reach (B) phases of motion. The path circuity for the withdraw (C) and reach (D) phases of the contralateral forepaw (*, $p<0.05$). Delta change of the path circuity for the withdraw and reach phases of each forelimb (E-H). Each dot on the graphs represents an individual animal.

Bimanual coordination was also measured to determine the synchrony of movement between the ipsilateral and contralateral forepaws. No changes in bimanual coordination were observed for both experimental groups and for the reach and withdraw phases of movement (Figure 11A-B). This was further corroborated by the delta change analysis of the bimanual coordination (Figure 11C-D).

Overall, from the 5 DLC analyses performed, only the movement scaling and path circuity for the contralateral forepaw of the withdraw and reach phases showed significant decreases in sham performance pre versus 2 days after sham surgery. This was unexpected given that over time we would not expect sham mice to have significant differences in kinematic measures. However, kinematic performances of sham and stroke mice were not different for any outcome measures. These findings do not align with the published kinematic deficits detected in injured rats performing the string-pull task ((Blackwell et al., 2018b), which could be due to a variety of differences between the study design, or possibly between species.

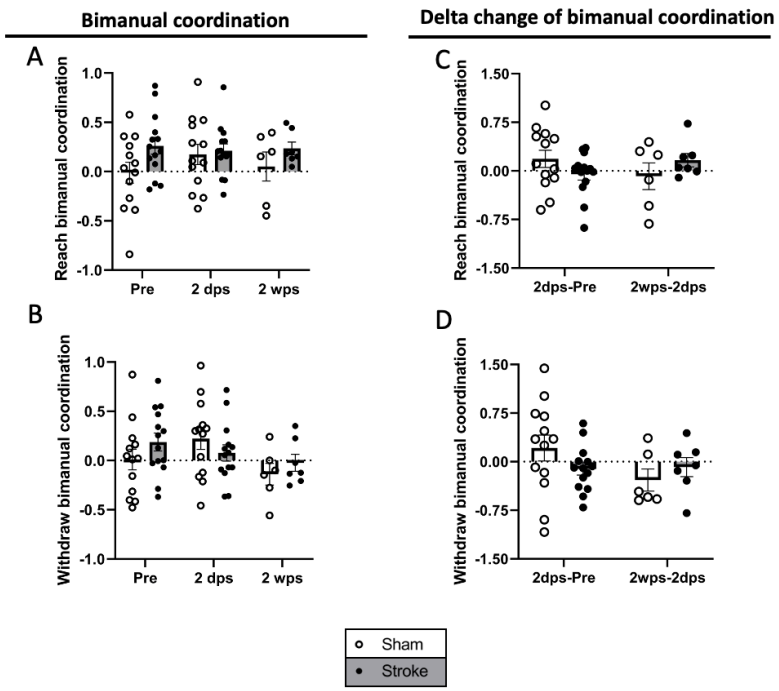

Figure 11: The bimanual coordination of sham and stroke mice are not different. The bimanual coordination of the withdraw (A) and the reach (B) phases. The delta change analysis of the bimanual coordination (C-D). Each dot on the graphs represents an individual animal.

4.3 Stroke Infarct Location and Volume

In alignment with the coordinates of the laser used to induce the stroke, the lesions were primarily in the M1, and little tissue damage was detected in the M2, as shown in Figure 12A-B. On average, the range of the infarcts spanned -0.1 to 1.8 mm from bregma. The stroke volumes at 2 dps were approximately 4 mm^3, compared to 1 mm^3 at 2 wps (Figure 12C-D). These findings align with the work of others, which have also shown that stroke lesions reduce in volume over time (Labat-gest and Tomasi, 2013).

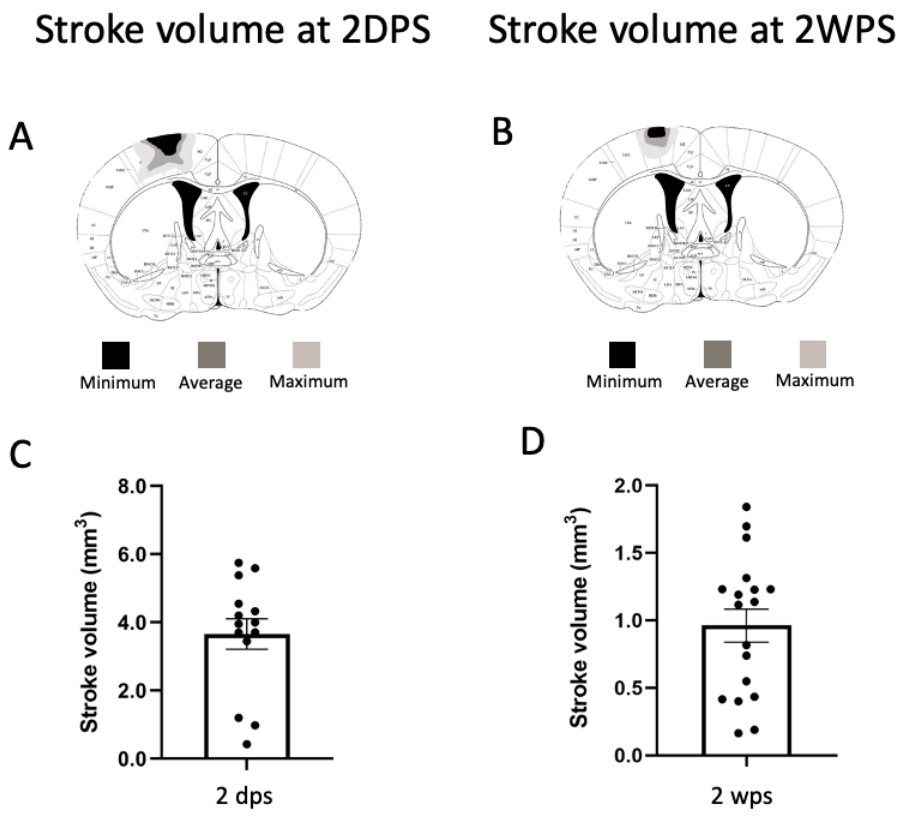

Figure 12: Photothrombotic stroke lesions. Schematic representation of the location of the stroke lesions for mice perfused at 2 dps (A) and 2 wps (B) respectively. Quantification of the stroke volume in mm^3 at 2 dps (C) and 2 wps (D). Each dot on the graphs represents an individual animal.

4.4 Less Activated Cells are Labelled in the Ipsilesional M2 of Stroke Mice at the Pre-Stroke Baseline Compared to 2 dps

To identify the motor networks used during the execution of the string-pulling task prior to the stroke compared to 2 days after a stroke, the number of YFP+ and c-Fos+ cells were measured respectively in the M2. The numbers of YFP+ cells were consistent in the contralesional and ipsilesional cortex of sham and PT stroke mice, suggesting that similar numbers of cells were active when performing the string-pull task prior to surgeries (Figure 13A-E). In contrast, the number of c-Fos+ cells at 2 dps were significantly different between the sham and stroke mice ($F_{(1, 48)} = 6.048$, $p=0.0176$), between the hemispheres ($F_{(1, 48)} = 6.520$, $p=0.0139$), and there was also a trend towards a significant interaction effect ($F_{(1, 48)} = 2.936$, $p=0.0931$) (Figure 13J). Post-hoc analysis showed a significant decrease in c-Fos+ cells in the ipsilesional hemisphere compared to contralesional cortex of stroke mice. Sham mice had no differences in the number of c-Fos+ cells between cortical hemispheres, with the number of c-Fos+ cells being similar to those in the contralesional hemisphere of stroke mice (Figure 13F-J). Furthermore, the number of reactivated cells pre-stroke and at 2 dps was assessed by the number of cells expressing both YFP and c-Fos. This analysis revealed that approximately 40% of cells were reactivated with no significant differences between the hemispheres nor between the sham and stroke mice (Figure 13K-O). Overall, these findings suggest that there is a decrease in the number of active cells in the ipsilesional M2 at 2 dps, which is accompanied by the same proportion of cells reactivated in both hemispheres as well as in the sham and stroke mice at 2 dps.

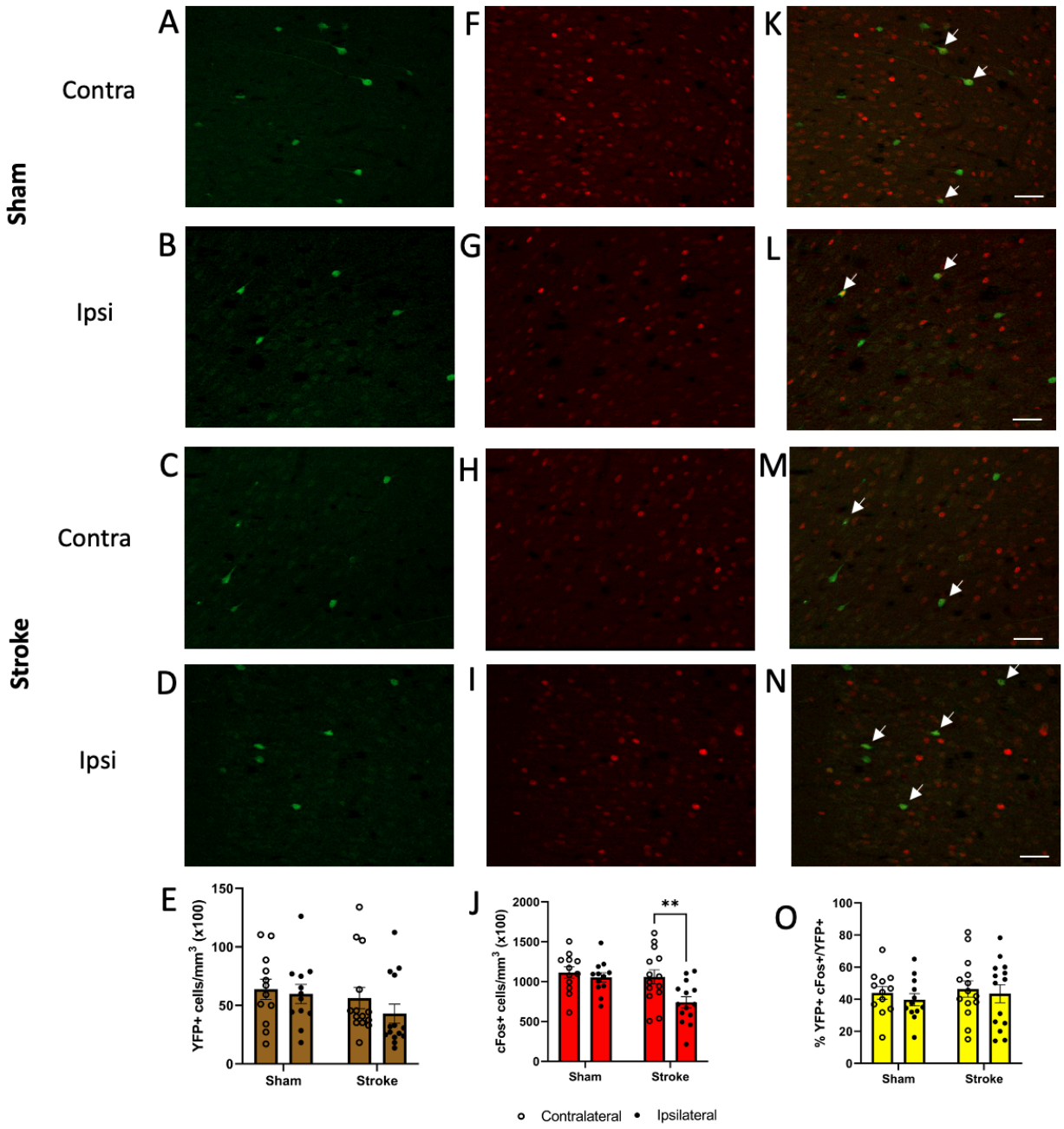

Figure 13: Decrease in active cells in the ipsilesional M2 of stroke mice at 2 dps. Representative images of both M2 motor cortices (contra: contralesional and ipsi: ipsilesional) for active cells pre-stroke (A-D), 2 wps (F-I) and cells active at both time points (K-N). Quantification of active cells at the pre-stroke baseline (E), 2 dps (J) and reactivated cells (O). Arrow heads indicate reactivated cells (cell expressing both YFP and c-Fos). Each dot on the graphs represents an individual animal. Error bar is 50 µm (**, $p<0.01$).

4.5 No Difference in Active or Reactivated Cells at 2 dps Compared to 2 wps

To identify the motor network used during the execution of the string-pulling task the number of YFP+ and c-Fos+ cells were measured in the M2 at 2 dps compared to 2 wps, respectively. The number of YFP+ cells were similar for both hemispheres of sham and stroke mice, suggesting that there was no change in the number of active cells 2 dps (Figure 14A-E). This was unexpected, since it directly contrasts findings reported in Figure 13J, in which the number of c-Fos+ cells were reduced in the ipsilesional M2 of stroke mice at 2 dps. We suspect that these differences may be attributed to differences in the magnitude of YFP+ versus c-Fos+ cells that are detected in the TRAP models, as discussed below. Examination of the number of c-Fos+ cells showed no differences between groups or hemispheres (Figure 14F-J). Also, 40% of cells were reactivated at 2 dps and 2 wps, in both the sham and stroke groups (Figure 14K-O). Overall, these findings suggest that at 2 dps versus 2 wps, there is no differences in the number of activated or reactivated cells in stroke or sham mice.

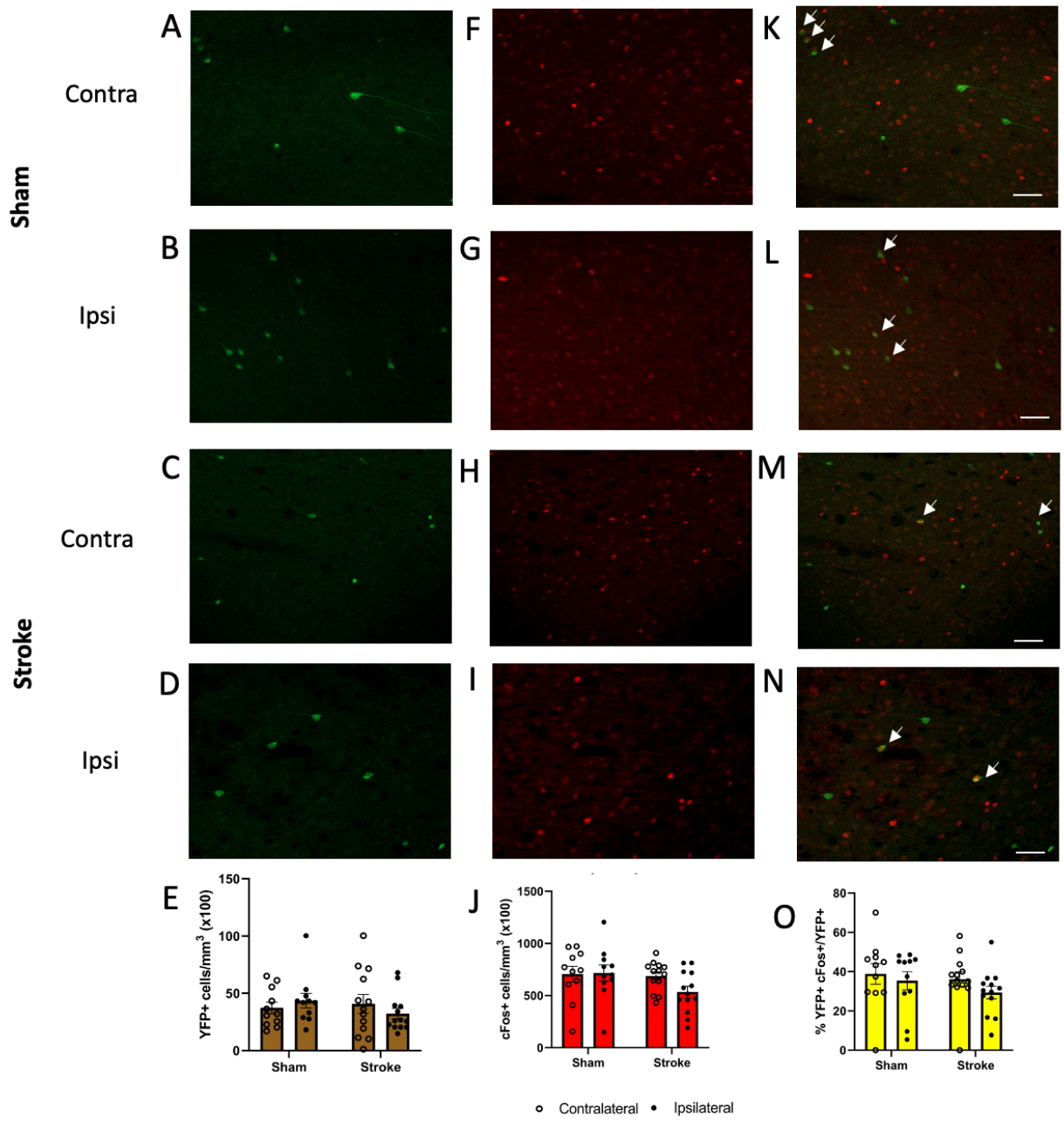

Figure 14: No differences in active or reactivated cells at 2 dps compared to 2 wps for sham and stroke mice. Representative images of both M2 motor cortices (contra: contralesional and ipsi: ipsilesional) for cell active at 2 dps (A-D), 2 wps (F-I) and cells active at both time points (K-N). Quantification of active cells at 2 dps (E), at 2 wps (J) and reactivated cells (O). Arrow heads indicate reactivated cells (cell expressing both YFP and c-Fos). Each dot on the graphs represents an individual animal. Error bar is 50 μm.

4.6 No Difference in Active or Reactivated Cells at the Pre-Stroke Baseline Compared to 2 wps

To identify the motor network used during the execution of the string-pulling task before and at 2 wps, the number of YFP+ and c-Fos+ cells were measured respectively. Both stroke and sham mice had similar numbers of activated YFP+ cells in both hemispheres at baseline (Figure 15A-E). Thus, this data replicates the results presented in Figure 13E. At 2 wps there was no difference in the number of activated c-Fos+ cells in the contra- and ipsilesional hemispheres of control and stroke mice (Figure 15F-J), which also replicates findings shown in Figure 14J. Furthermore, between 50-60% of cells active at baseline were reactivated at 2 wps (Figure 15K-O). Altogether these results combined with previous experiments, suggest that stroke and sham mice have similar numbers of activated and reactivated cells at the pre-stroke baseline and at 2 wps.

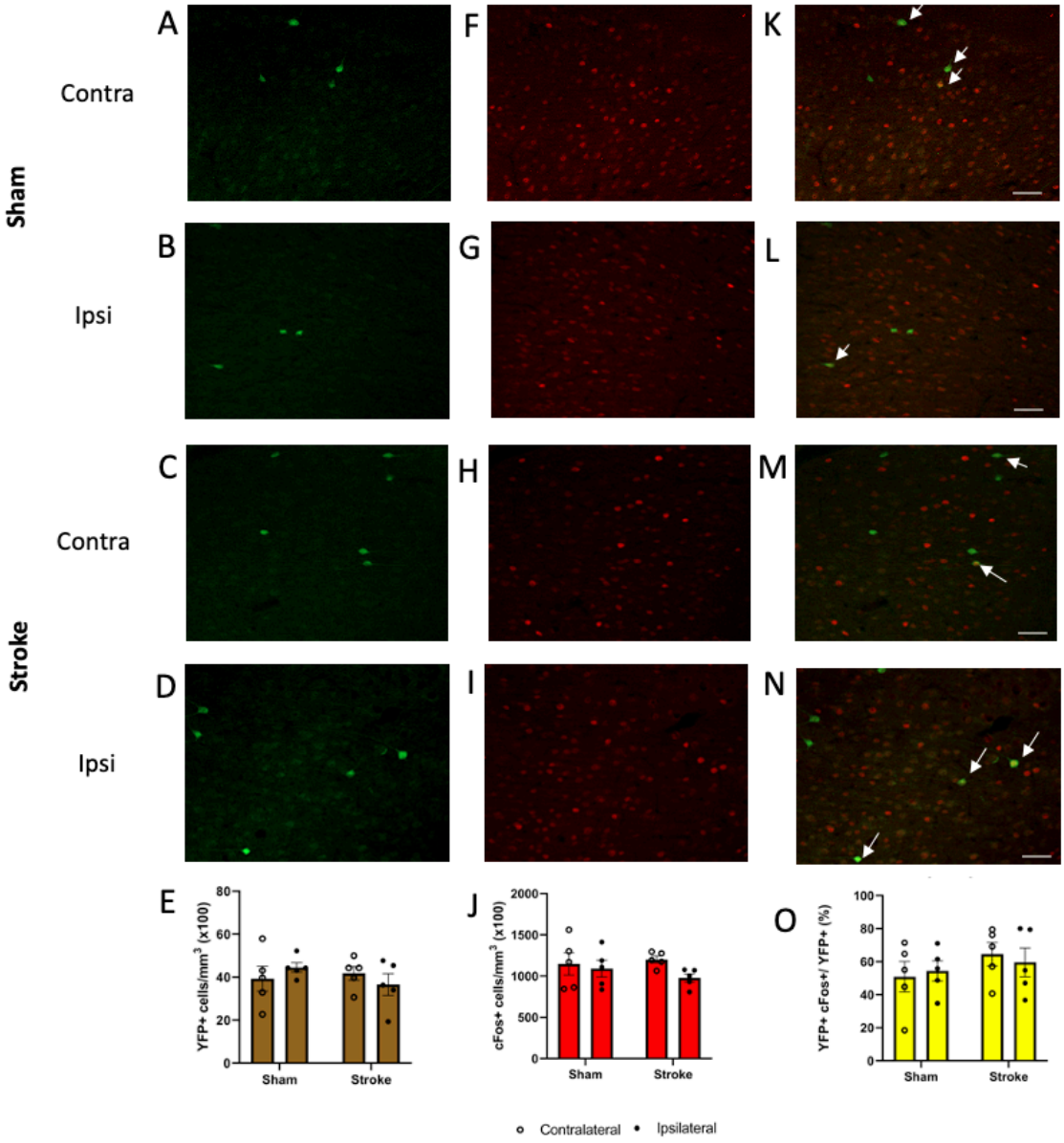

Figure 15: No differences in active or reactivated cells before the stroke and at 2 wps for sham and stroke mice. Representative images of both M2 motor cortices (contra: contralesional and ipsi: ipsilesional) for cell active pre-stroke (A-D), 2 wps (F-I) and cells active at both time points (K-N). Quantification of cells active pre-stroke (E), at 2 wps (J) and reactivated cells (O). Arrow heads indicate reactivated cells (cell expressing both YFP and c-Fos). Each dot on the graphs represents an individual animal. Error bar is 50 μm.

4.7 Less Active Cells in Sham and Stroke Mice Express NeuN Following Surgeries

To assess if the activated cells from all three different experimental designs (Figure 4) had a neuronal phenotype, we determined if the activated cells expressed the pan-neuronal marker, NeuN (Gusel'nikova and Korzhevskiy, 2015). At baseline, approximately 90% or more of YFP+ cells co-expressed NeuN in the sham and stroke mice, with no differences between the hemispheres (Figure 16A-C). At 2dps, ~60% of activated cells that were labeled with either YFP or c-Fos co-expressed NeuN, with no differences between groups nor between hemispheres (Figure 16D-E). Similarly, at 2 wps, ~60% of cells labeled with either YFP or c-Fos were co-labelled with NeuN, independent of the groups or hemispheres (Figure 16G-I). Altogether, these findings unexpectedly show that both sham and stroke mice have an approximately 20% decrease in NeuN+ cells following surgeries. Future work will need to be conducted to assess whether IEG expressing cells are astrocytes or other cells, and why sham and stroke mice both show a decrease in NeuN expression post-surgeries.

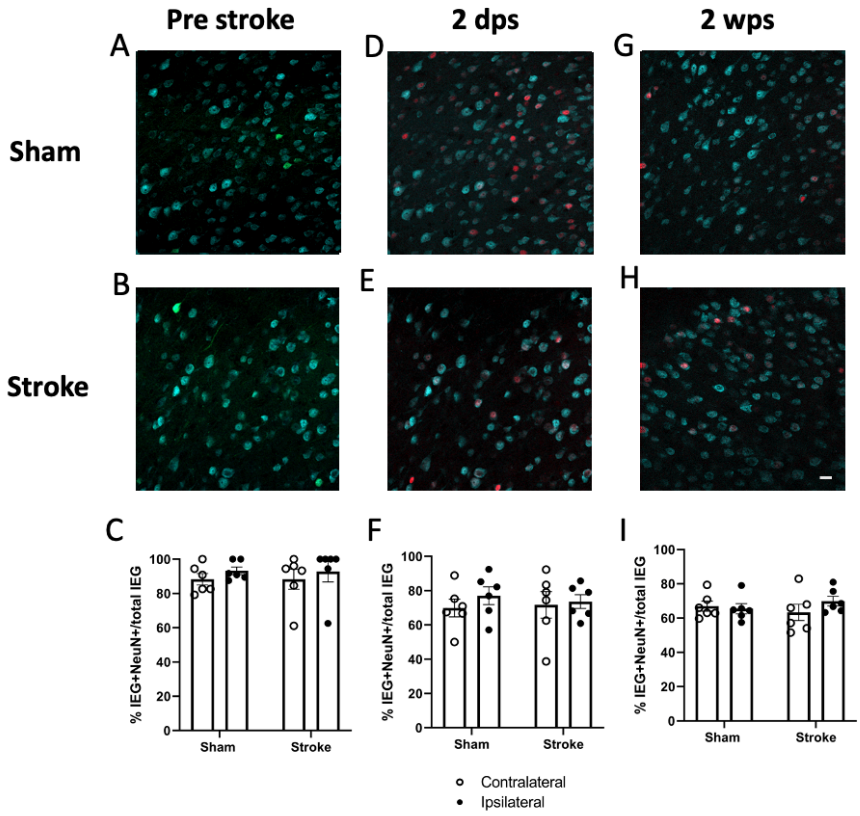

Figure 16: Irrelevant of stroke injuries, less IEG+ cells are co-labeled with NeuN. Representative images from the ipsilesional M2 of sham (A,D,G) and stroke (B,E,H) mice at the pre-stroke (A,B), 2 dps (D,E) and 2 wps (G,H) time points. In the representative images, YFP is green, cFos is red and NeuN is blue. Quantification of colocalized IEG+ cells with NeuN at baseline (C), 2 dps (F) and 2 wps (I). Each dot on the graphs represents an individual animal. The scale bar is 20 μm.

5. Discussion

Cortical remapping has been extensively shown in both clinical and preclinical models of stroke recovery. Despite this evidence, whether motor networks remain stable throughout stroke recovery, specifically whether the same or different cells are utilized when performing a behavioural task remain unknown. This thesis used the Arc-TRAP model to examine the number of cells activated during the string-pulling behaviour following a photothrombotic stroke. Stroke mice had a significant decline in the amount of string pulled when assessed 2 days after the stroke in the absence of differences in kinematic movements used to perform the task, as assessed by DLC analysis. This decline in behavioural performances was accompanied by a significant decrease in the number of active cells in the ipsilesional M2 cortex. In contrast, 2 weeks after the stroke, there were improvements in string-pull performance, as well as no significant differences in the number of active cells in stroke and sham mice. Additionally, around 40% of cells were reactivated at either 2 days or 2 weeks after stroke compared to the pre-stroke baseline for all mice. Phenotyping of active cell for both sham and stroke mice revealed that prior to the surgeries ~90% of active cells expressed the neuronal marker NeuN, while after the sham and stroke surgery,~60 % of active cells were NeuN+. Overall, this work demonstrates that mice pull less string acutely after stoke (2dps), which is associated with less active cells in the ipsilesional M2, however, there is no change in the proportion of reactivated cells used after a stroke when performing the string-pull task.

5.1 M2 Networks Remain Stable Throughout Stroke Recovery Despite Decreases in Active Cells at 2 dps

Our results, which demonstrate that fewer cells are active in the injured hemisphere at 2 dps, corroborate previous work published by Dr. Tim Murphy's Laboratory (Brown et al., 2009; Lim et al., 2014; Mohajerani et al., 2011). These studies demonstrated that changes in cortical

activity and sensorimotor maps of the stroke injured hemisphere can occur within hours following a stroke and suggest that these disruptions in activity can last up to 1 week after the stroke injury in the ipsilesional cortex Additionally, they showed that by 8 weeks post-stroke remapping of the sensory and motor networks was restored within the ipsilesional M1 region (Brown et al., 2009; Lim et al., 2014). This finding aligns with our result that showed at 2 wps there was no differences in the number of active cells in the ipsilesional M2 of sham and stroke mice. Altogether, these findings suggest that stroke induces an acute reduction in ipsilesional M1 and M2 activity when performing a motor task, however during recovery, this activity is restored.

Our interpretation of there being less cell active in the ipsilesional M2 cortex at 2 dps is based on our examination of the number the c-Fos+ cells at 2 dps (Figure 13 (Pre versus 2 dps experiment)). As noted in the result section, this finding was contradicted by a lack of a similar reduction in YFP+ cells at 2 dps in the 2 days versus 2 wps experiment (Figure 14). It is also notable that the number of YFP+ and c-Fos+ cells quantified at 2 dps in these two experiments was very different: ~5 000 YFP+ cells/mm^3 (Figure 14) versus ~90 000 c-Fos+ cells/mm^3 (Figure 13). This ~20-fold difference in labelled YFP versus c-Fos cells has also previously been reported in the characterization of the Arc-TRAP model (Denny et al., 2014), and to a lesser extent, in the c-Fos TRAP literature (Hwang et al., 2022; Ivashkina et al., 2021). Differences in Arc and c-Fos expression within cells is one possible explanation for why Arc-TRAP models labelled more c-Fos+ then Arc+ cells. However, previous work from Marc Vani's thesis (Vani, 2018) demonstrated that ~ 95% of cells that express the Arc protein also express the c-Fos protein. This data suggests that the difference in the number of YFP+ versus c-Fos+ cells is not due to differences in the expression of Arc versus c-Fos within cells. Instead, it seems more likely that

the recombination efficiency of the TRAP model to label Arc+ cells with YFP may be causing this difference, which could be tested in future studies.

Throughout all of our experiments, the number of active cells in the contralesional hemisphere remained consistent and did not change when there was a reduction in the number of active cells within the ipsilesional cortex (Figure 13-15). This finding is in alignment with work from Johnston et al. (2013), that reported no change in functional remapping in the forepaw sensory representation of the contralesional hemisphere up to 4 weeks following either a PT or MCAO-induced stroke in juvenile and adult mice. However, these findings also contrast other studies in the field (Dijkhuizen et al., 2003; Jablonka et al., 2010; Jones and Adkins, 2015; Mohajerani et al., 2011; Takatsuru et al., 2009). For example, previous work has demonstrated that acutely following a PT-induced stroke (~30 minutes), there is an increase in the activity of the contralesional hemisphere in mice (Mohajerani et al., 2011). Increased activity of the contralesional hemisphere was also reported 1- and 3-days after a unilateral middle cerebral artery occlusion (MCAO) using fMRI in rats, and as early as 1 day following a PT induced stroke in rats (Dijkhuizen et al., 2003; Jablonka et al., 2010). Takatsuru and colleagues (2009) further demonstrated increases in neuronal activity in the contralesional hemisphere within 2 days to 1 week following PT strokes in mice. These findings also collaborate the clinical literature that has shown the bilateral activation of the contralesional hemisphere during stroke recovery (Bütefisch et al., 2005; Rehme et al., 2011; Ward et al., 2003).

We hypothesize that there were no observed changes in contralesional activity due to differences in the experimental design between our work and the work of others. For example, bi-hemispheric activity was measured following the stimulation of the forepaws of animals and whisker stimulation in previous studies (Dijkhuizen et al., 2003; Jablonka et al., 2010; Mohajerani

et al., 2011), while in our study, cells recruited during the performance of the motor string-pull behavioural task were labelled. Furthermore, the location of the strokes are different between our work and others. As noted in the introduction, most studies focused their work on the M1 sensory-motor cortex (Brown et al., 2009; Lim et al., 2014; Mohajerani et al., 2011), and to our knowledge, we are the first group to assess reorganization in the intact M2 following a stroke localized to the M1. Previous work from Harrison et al. (2013) has examined the effect of photothrombotic strokes of similar volumes in different cortical regions on cortical reorganization. This work showed that when strokes were administered in the sensory areas, the sensory maps were shifted toward the primary motor cortex. However, when strokes were administered in the motor regions, the centre of the motor maps remained unaltered, while its distribution was more diffused. Thus, stroke volumes and location may alter the degree and the properties of cortical reorganization. This highlights the need to further characterize if and how cortical remapping takes place following strokes of varying sizes and location across all other cortical regions. In this regard, future work using brain clearing methodology could be used to assess brain wide changes in cellular activity, as previously done using the CLARITY methods with the ARC-TRAP mice (Ye et al., 2016).

The only other group that has used a TRAP model to assess reorganization following a stroke, used the cFos-CreER^{T2}:Ai9 mice, as well as intrinsic signal and *in vivo* calcium imaging (Zeiger et al., 2021). This study showed no evidence of remapping within adjacent and surviving regions of the C1 barrel in the barrel field of the primary somatosensory cortex following a PT stroke to the C1 barrel cortex. From 5 days, up to 2 months following the stroke, they found no increases in the number of C1 whisker responsive neurons in the spared neighboring barrels. This finding is in alignment with our consistent ~40% of reactivated cells being used when the mice performed the string-pull task before or after stroke, in either hemisphere and in both the sham and

stroke mice. These findings are also in alignment with another study that demonstrated that ~40% of cells were reactivated in the M1 of naïve c-Fos TRAP mice that learned the forelimb reaching task (Hwang et al., 2022). Altogether, these studies support our work and suggest that the cell networks used to perform the string-pull tasks may not change in the M2 cortex following a stroke.

Using the cFos-CreER^{T2}:Ai9 mice, Zeiger et al. (2021) also observed that forced use whisker therapy was able to potentiate sensory-evoked responses in surround whisker neurons, but this did not result in true circuit remapping with the recruitment of new C1 whisker responsive neurons. Since our work did not complete any measures of activity within the labeled neurons, it is possible that the activity of neurons is increased in the contralesional and ipsilesional hemisphere, as opposed to more cells being recruited to the motor cortices post-stroke and throughout recovery. Thus, it would be interesting in future studies to test if the M2 cortices of the Arc-TRAP mice have any differences in sensory-dependent responses.

5.2 Phenotype of Arc-TRAP and IHC Labelled Cells

When examining the phenotype of the cells activated by the string-pull task, as expected at baseline for both the sham and stroke mice, the majority (~90%) of active cells expressed the pan-neuronal NeuN marker in both hemispheres. This is in accordance with the literature reporting that IEGs are selectively and rapidly upregulated in response to insults or neuronal activity (Minatohara et al., 2015; Zukin et al., 2004). Specifically, Arc is well known to be a master regulator of synaptic plasticity mediating stable long-term potentiation and long-term depression in neurons, while c-Fos dimerizes with proteins of the JUN family to form the transcription factor complex AP-1 following neuronal activity (Gallo et al., 2018; Nikolaienko et al., 2018). At 2 dps and 2 wps, it was unexpected to observe a 20% reduction in NeuN expression in the active Arc and c-Fos labelled cells in both the stroke and sham control mice. This result does not seem to be

a simple effect of damage or cell death, since cresyl violet staining confirmed that strokes were restricted to the ipsilesional cortex of stroke mice. Although IEGs are most often reported to be expressed in neurons, glial cells have been reported to express IEGs (Rodríguez et al., 2008). For example, Jiang and VanDongen (2020) have shown a neuronal activity dependent accumulation of Arc within astrocytes in naïve mice. Furthermore, in accordance with some of our findings, previous studies on the central and peripheral nervous system have demonstrated that damaged neurons can decrease their expression of NeuN (Darlot et al., 2017; Hernandez et al., 2019; McPhail et al., 2004; Wu et al., 2010). Consequently, future work is required to determine the cellular phenotype of the active cells that did not express NeuN, which could be done by IHC staining for microglia, oligodendrocyte or astrocyte markers.

5.3 No Differences in Kinematic Performance Between Sham and Stroke Mice

Our findings also revealed that stroke mice pulled less string compared to sham controls at 2 dps on the bimanual string-pulling task. The stroke mice had begun to recover by 2 weeks after stroke, as shown by their increase amount of string pulled, albeit this increase did not attain the pre-stroke baseline value. This finding corroborates other behavioural recovery profiles in mice, which show that SBR of motor functions can occurs within weeks of a stroke (Karthikeyan et al., 2019). In contrast to the stroke group, sham mice gradually pulled less string over the 2 weeks following surgeries. This unexpected reduction in string-pulling behaviour was not previously observed by the Blackwell group that established the string-pull protocol for rats and mice, however, their protocol includes a reward system to motivate string-pulling behaviour (Blackwell et al., 2018b). Specifically, they showed that mice trained with a higher reinforcement frequency protocol (more strings with cashews), increased by approximately 2 folds the amount of string pulled by mice (Blackwell and Wallace, 2020). Although these findings suggest that adding

cashews to the string may entice the mice to pull more string, we did not include food rewards due to concerns about activity induced by mastication and the reward. Altogether, our findings suggest that despite sham mice becoming less motivated to pull as much string at later time points, the string-pull task successfully assessed stroke deficits.

In addition to measuring the amount of string pulled by mice, DLC was used to kinematically measure the efficiency in the movements employed throughout the string-pull motion. This analysis showed that sham and stroke mice had similar movements patterns when performing the string-pull task. This was unexpected given that the only other study performing kinematic analysis with the string-pull task found that the rhythmicity of movement in rats was disrupted early post injury and restored within a month (Blackwell et al., 2018b). Additionally, our laboratory had previously found kinematic deficits in mice after a PT-induced stroke when performing the staircase task (Balbinot et al., 2022). These results suggest that the mice have no kinematic deficits following stroke when performing the string-pull task, however this result could also be due to the protocol that we used to detect kinematic movements throughout the string-pull behaviour.

To further help determine if sham and PT stroke mice have any significant differences in movements employed during the string-pull test, there are a variety of modifications that could be applied in future studies to the DLC and kinematic analysis protocols. One aspect of the analysis that could be refined is how the pulling motion is separated into different reach and withdrawal phases. In this analysis, the reach and withdraw phases were defined as either the upward or downward movement of the forepaws, respectively. This definition therefore does not account for the differences in paw movements within each of these phases. Blackwell et al. (2018a) accounted for the variability during the reach and withdraw phases in mice by subdividing the movements

into 5 distinct phases; 1) lift (first upward movement), 2) advance (paw is approaching the string), 3) grasp, 4) pull (first downward movement) and 5) push (second downward movement when the mice are pushing on the string). This subdivision of the movement phases led to the identification that the lift and advance movements were more rapid than the grasp, pull and push phases. Furthermore, horizontal directional changes were present at the pull/push transition. Therefore, to increase our ability to measure changes in movements during the string-pulling motion following a stroke, the reach and withdraw phases may need to be subdivided into the 5 specific phases. A second modification that could be employed in the protocol, would be to perform 3D instead of 2D joint movements analyses. Recently, 3D limb trajectory tracking systems based on actual 3D joint locations have been made readily available for the neuroscience community and show high labelling efficiency (Arac et al., 2019; Veronika et al., 2022). Arac et al. (2019) have specifically described how to implement 3D kinematic analyses on commonly used behavioural tasks in the field of neuroscience, such as the skilled pellet reaching task. 3D reconstruction of movement can be obtained using 2 front and side facing high-speed cameras along with a camera calibration tool which creates a 3D cartesian coordinate system and provides 3D paw positions from the 2 camera views. Thus, in future studies, the implementation of the movement phase subdivisions and 3D analyses would be useful to gain insight into the naturalistic movements performed during the string-pulling task and further assess if there are fine motor impairments following a stroke.

6. Conclusions

The findings from this thesis demonstrate that 2 days after a PT-induced stoke, Arc-TRAP stroke mice pull less string and have a reduction in the number of active cells in their ipsilesional M2 cortex compared to sham mice. No change in number of active cells in contralesional cortex were observed and approximately 40% of cells that were used prior to stroke were reactivated acutely after stroke. By 2 weeks post-stroke, the mice displayed a significantly increase in the amount of string pulled, which was accompanied by no differences in the number of active, or reactivated cells in the ipsilesional or contralesional cortex. We further reported that irrelevant of stroke injury, both stroke and sham mice had less NeuN+ and IEG expressing cells post-surgery. Thus, this work demonstrates that there is an acute reduction in the number of active cells in the ipsilesional cortex after stroke that is accompanied by a significant reactivation of a proportion of the initial motor networks used to perform the string-pull task following a stroke and throughout recovery.

Supplemental figure

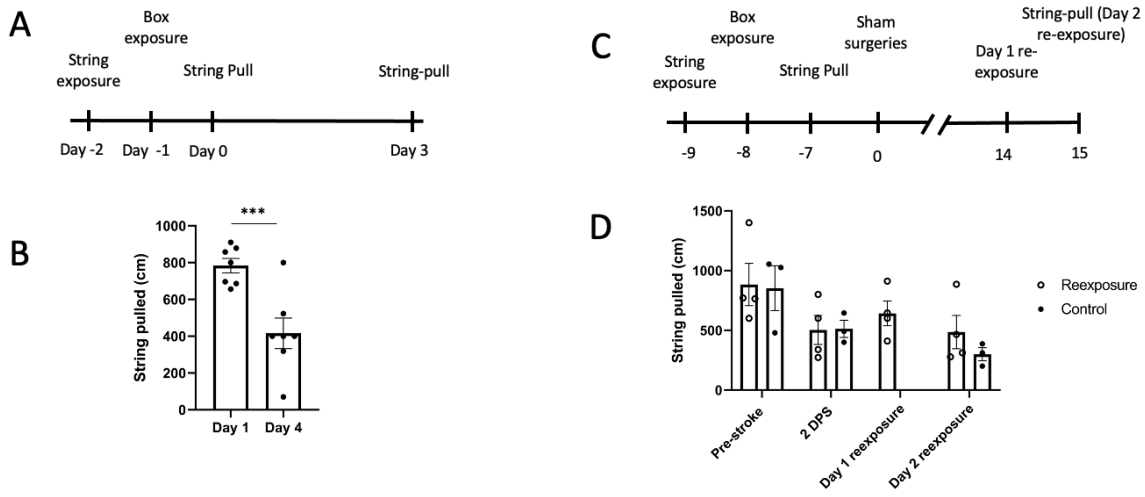

Supplemental figure 1: Re-exposure is insufficient to increase the amount of string pulled overtime. (A) Behavioural time line used to assess if naïve mice pulled less string overtime. (B) The amount of string pulled by naïve mice (***, $p<0.001$). C) Behavioural time line used to assess the effect of re-exposure on string pulling. D) The amount of string pulled in cm following string-pull re-exposure. Each dot on the graphs represents an individual animal.

7. References

AHA, 2022, About stroke, *in* A. S. Association, ed., Online, American Heart Association.

Arac, A., P. Zhao, B. H. Dobkin, S. T. Carmichael, and P. Golshani, 2019, DeepBehavior: A Deep Learning Toolbox for Automated Analysis of Animal and Human Behavior Imaging Data: Frontiers in systems neuroscience, v. 13, p. 20-20.

Balbinot, G., S. Denize, and D. C. Lagace, 2022, The Emergence of Stereotyped Kinematic Synergies when Mice Reach to Grasp Following Stroke: Neurorehabilitation and neural repair, v. 36, p. 69-79.

Bernhardt, J., K. S. Hayward, G. Kwakkel, N. S. Ward, S. L. Wolf, K. Borschmann, J. W. Krakauer, L. A. Boyd, S. T. Carmichael, D. Corbett, and S. C. Cramer, 2017, Agreed definitions and a shared vision for new standards in stroke recovery research: The Stroke Recovery and Rehabilitation Roundtable taskforce: Int J Stroke, v. 12, p. 444-450.

Biernaskie, J., A. Szymanska, V. Windle, and D. Corbett, 2005, Bi-hemispheric contribution to functional motor recovery of the affected forelimb following focal ischemic brain injury in rats: The European journal of neuroscience, v. 21, p. 989-999.

Billinger, S. A., R. Arena, J. Bernhardt, J. J. Eng, B. A. Franklin, C. M. Johnson, M. MacKay-Lyons, R. F. Macko, G. E. Mead, E. J. Roth, M. Shaughnessy, and A. Tang, 2014, Physical activity and exercise recommendations for stroke survivors: a statement for healthcare professionals from the American Heart Association/American Stroke Association: Stroke, v. 45, p. 2532-53.

Binder, E., M. Leimbach, E. M. Pool, L. J. Volz, S. B. Eickhoff, G. R. Fink, and C. Grefkes, 2021, Cortical reorganization after motor stroke: A pilot study on differences between the upper and lower limbs: Human brain mapping, v. 42, p. 1013-1033.

Blackwell, A. A., M. T. Banovetz, Qandeel, I. Q. Whishaw, and D. G. Wallace, 2018a, The structure of arm and hand movements in a spontaneous and food rewarded on-line string-pulling task by the mouse: Behav Brain Res, v. 345, p. 49-58.

Blackwell, A. A., and D. G. Wallace, 2020, Effects of string length on the organization of rat string-pulling behavior: Anim Cogn, v. 23, p. 415-425.

Blackwell, A. A., W. L. Widick, J. L. Cheatwood, I. Q. Whishaw, and D. G. Wallace, 2018b, Unilateral forelimb sensorimotor cortex devascularization disrupts the topographic and kinematic characteristics of hand movements while string- pulling for food in the rat: Behav Brain Res, v. 338, p. 88-100.

Bowman, H., A. Bonkhoff, T. Hope, C. Grefkes, and C. Price, 2021, Inflated Estimates of Proportional Recovery From Stroke: The Dangers of Mathematical Coupling and Compression to Ceiling: Stroke (1970), v. 52, p. 1915-1920.

Brecht, M., A. Krauss, S. Muhammad, L. Sinai-Esfahani, S. Bellanca, and T. W. Margrie, 2004, Organization of rat vibrissa motor cortex and adjacent areas according to cytoarchitectonics, microstimulation, and intracellular stimulation of identified cells: J Comp Neurol, v. 479, p. 360-73.

Brown, C. E., K. Aminoltejari, H. Erb, I. R. Winship, and T. H. Murphy, 2009, In vivo voltage-sensitive dye imaging in adult mice reveals that somatosensory maps lost to stroke are replaced over weeks by new structural and functional circuits with prolonged modes of activation within both the peri-infarct zone and distant sites: J Neurosci, v. 29, p. 1719-34.

Brown, C. E., P. Li, J. D. Boyd, K. R. Delaney, and T. H. Murphy, 2007, Extensive turnover of dendritic spines and vascular remodeling in cortical tissues recovering from stroke: J Neurosci, v. 27, p. 4101-9.

Bütefisch, C. M., R. Kleiser, B. Körber, K. Müller, H. J. Wittsack, V. Hömberg, and R. J. Seitz, 2005, Recruitment of contralesional motor cortex in stroke patients with recovery of hand function: Neurology, v. 64, p. 1067-1069.

Cao, V. Y., Y. Ye, S. Mastwal, M. Ren, M. Coon, Q. Liu, R. M. Costa, and K. H. Wang, 2015, Motor Learning Consolidates Arc-Expressing Neuronal Ensembles in Secondary Motor Cortex: Neuron, v. 86, p. 1385-92.

Cheng, N. T., and A. S. Kim, 2015, Intravenous Thrombolysis for Acute Ischemic Stroke Within 3 Hours Versus Between 3 and 4.5 Hours of Symptom Onset: Neurohospitalist, v. 5, p. 101-109.

Chwastek, D., 2019, Differential cellular reactivation occurs post-stroke during motor behaviour, uOttawa.

Cortes-Perez, I., F. A. Nieto-Escamez, and E. Obrero-Gaitan, 2020, Immersive Virtual Reality in Stroke Patients as a New Approach for Reducing Postural Disabilities and Falls Risk: A Case Series: Brain Sci, v. 10.

Coupar, F., A. Pollock, P. Rowe, C. Weir, and P. Langhorne, 2012, Predictors of upper limb recovery after stroke: a systematic review and meta-analysis: Clinical rehabilitation, v. 26, p. 291-313.

Darlot, F., S. Vinit, V. Matarazzo, and A. Kastner, 2017, Sustained cell body reactivity and loss of NeuN in a subset of axotomized bulbospinal neurons after a chronic high cervical spinal cord injury: The European journal of neuroscience, v. 46, p. 2729-2745.

De Bruyn, N., S. Meyer, S. S. Kessner, B. Essers, B. Cheng, G. Thomalla, A. Peeters, S. Sunaert, T. Duprez, V. Thijs, H. Feys, K. Alaerts, and G. Verheyden, 2018, Functional network connectivity is altered in patients with upper limb somatosensory impairments in the acute phase post stroke: A cross-sectional study: PloS one, v. 13, p. e0205693-e0205693.

Denny, C. A., M. A. Kheirbek, E. L. Alba, K. F. Tanaka, R. A. Brachman, K. B. Laughman, N. K. Tomm, G. F. Turi, A. Losonczy, and R. Hen, 2014, Hippocampal memory traces are differentially modulated by experience, time, and adult neurogenesis: Neuron, v. 83, p. 189-201.

Dijkhuizen, R. M., A. B. Singhal, J. B. Mandeville, O. Wu, E. F. Halpern, S. P. Finklestein, B. R. Rosen, and E. H. Lo, 2003, Correlation between Brain Reorganization, Ischemic Damage, and Neurologic Status after Transient Focal Cerebral Ischemia in Rats: A Functional Magnetic Resonance Imaging Study: The Journal of neuroscience, v. 23, p. 510-517.

Duan, C. A., Y. Pan, G. Ma, T. Zhou, S. Zhang, and N. L. Xu, 2021, A cortico-collicular pathway for motor planning in a memory-dependent perceptual decision task: Nat Commun, v. 12, p. 2727.

Ergul, A., A. Alhusban, and S. C. Fagan, 2012, Angiogenesis A Harmonized Target for Recovery After Stroke: Stroke (1970), v. 43, p. 2270-2274.

Farris, S., G. Lewandowski, C. D. Cox, and O. Steward, 2014, Selective localization of arc mRNA in dendrites involves activity- and translation-dependent mRNA degradation: The Journal of neuroscience, v. 34, p. 4481-4493.

Fleet, A., S. J. Page, M. MacKay-Lyons, and S. G. Boe, 2014, Modified constraint-induced movement therapy for upper extremity recovery post stroke: what is the evidence?: Top Stroke Rehabil, v. 21, p. 319-31.

Gallo, F. T., C. Katche, J. F. Morici, J. H. Medina, and N. V. Weisstaub, 2018, Immediate Early Genes, Memory and Psychiatric Disorders: Focus on c-Fos, Egr1 and Arc: Frontiers in behavioral neuroscience, v. 12, p. 79-79.

Grefkes, C., and G. R. Fink, 2020, Recovery from stroke: current concepts and future perspectives: Neurological Research and Practice, v. 2, p. 17-17.

Grefkes, C., and N. S. Ward, 2014, Cortical Reorganization After Stroke: How Much and How Functional?: The Neuroscientist (Baltimore, Md.), v. 20, p. 56-70.

Guenthner, Casey J., K. Miyamichi, Helen H. Yang, H. C. Heller, and L. Luo, 2013, Permanent Genetic Access to Transiently Active Neurons via TRAP: Targeted Recombination in Active Populations: Neuron (Cambridge, Mass.), v. 79, p. 1257-1257.

Gusel'nikova, V. V., and D. E. Korzhevskiy, 2015, NeuN As a Neuronal Nuclear Antigen and Neuron Differentiation Marker: Acta Naturae, v. 7, p. 42-7.

Guzowski, J. F., B. Setlow, E. K. Wagner, and J. L. McGaugh, 2001, Experience-Dependent Gene Expression in the Rat Hippocampus after Spatial Learning: A Comparison of the Immediate-Early Genes Arc, c-fos, and zif268: The Journal of neuroscience, v. 21, p. 5089-5098.

Harrison, T. C., G. Silasi, J. D. Boyd, and T. H. Murphy, 2013, Displacement of sensory maps and disorganization of motor cortex after targeted stroke in mice: Stroke, v. 44, p. 2300-6.

Heart&Stoke, 2017, Different Strokes, Online, Heart & Stroke Foundation.

Hernandez, M. L., T. Chatlos, K. M. Gorse, and A. D. Lafrenaye, 2019, Neuronal Membrane Disruption Occurs Late Following Diffuse Brain Trauma in Rats and Involves a Subpopulation of NeuN Negative Cortical Neurons: Frontiers in neurology, v. 10, p. 1238-1238.

Hope, T. M. H., K. Friston, C. J. Price, A. P. Leff, P. Rotshtein, and H. Bowman, 2019, Recovery after stroke: not so proportional after all?: Brain (London, England : 1878), v. 142, p. 15-22.

Hwang, F.-J., R. H. Roth, Y.-W. Wu, Y. Sun, D. K. Kwon, Y. Liu, and J. B. Ding, 2022, Motor learning selectively strengthens cortical and striatal synapses of motor engram neurons: Neuron (Cambridge, Mass.), v. 110, p. 2790-2801.e5.

Ivashkina, O. I., A. M. Gruzdeva, M. A. Roshchina, K. A. Toropova, and K. V. Anokhin, 2021, Imaging of C-fos Activity in Neurons of the Mouse Parietal Association Cortex during Acquisition and Retrieval of Associative Fear Memory: International journal of molecular sciences, v. 22, p. 8244.

Jablonka, J. A., K. Burnat, O. W. Witte, and M. Kossut, 2010, Remapping of the somatosensory cortex after a photothrombotic stroke: dynamics of the compensatory reorganization: Neuroscience, v. 165, p. 90-100.

Jeffers, M. S., S. Karthikeyan, and D. Corbett, 2018, Does Stroke Rehabilitation Really Matter? Part A: Proportional Stroke Recovery in the Rat: Neurorehabilitation and neural repair, v. 32, p. 3-6.

Jeong, M., Y. Kim, J. Kim, D. D. Ferrante, P. P. Mitra, P. Osten, and D. Kim, 2016, Comparative three-dimensional connectome map of motor cortical projections in the mouse brain: Sci Rep, v. 6, p. 20072.

Jiang, Y., and A. M. J. VanDongen, 2020, Neuronal Activity-Dependent Accumulation of Arc in Astrocytes, bioRxiv.

Johansen-Berg, H., M. F. Rushworth, M. D. Bogdanovic, U. Kischka, S. Wimalaratna, and P. M. Matthews, 2002, The role of ipsilateral premotor cortex in hand movement after stroke: Proc Natl Acad Sci U S A, v. 99, p. 14518-23.

Johnston, D. G., M. Denizet, R. Mostany, and C. Portera-Cailliau, 2013, Chronic in vivo imaging shows no evidence of dendritic plasticity or functional remapping in the contralesional cortex after stroke: Cerebral cortex (New York, N.Y. 1991), v. 23, p. 751-762.

Johnston, S. C., 2002, Transient Ischemic Attack: The New England journal of medicine, v. 347, p. 1687-1692.

Jones, T. A., and D. L. Adkins, 2015, Motor System Reorganization After Stroke: Stimulating and Training Toward Perfection: Physiology (Bethesda), v. 30, p. 358-70.

Kannangara, T. S., A. Carter, Y. Xue, J. S. Dhaliwal, J. C. Beique, and D. C. Lagace, 2018, Excitable Adult-Generated GABAergic Neurons Acquire Functional Innervation in the Cortex after Stroke: Stem Cell Reports, v. 11, p. 1327-1336.

Karthikeyan, S., M. S. Jeffers, A. Carter, and D. Corbett, 2019, Characterizing Spontaneous Motor Recovery Following Cortical and Subcortical Stroke in the Rat: Neurorehabil Neural Repair, v. 33, p. 27-37.

Kessner, S. S., E. Schlemm, B. Cheng, U. Bingel, J. Fiehler, C. Gerloff, and G. Thomalla, 2019, Somatosensory Deficits After Ischemic Stroke: Time Course and Association With Infarct Location: Stroke (1970), v. 50, p. 1116-1123.

Khare, S., 2016, Risk factors of transient ischemic attack: An overview: Journal of mid-life health, v. 7, p. 2-7.

Krueger, H., J. Koot, R. E. Hall, C. O'Callaghan, M. Bayley, and D. Corbett, 2015, Prevalence of Individuals Experiencing the Effects of Stroke in Canada: Trends and Projections: Stroke (1970), v. 46, p. 2226-2231.

Kundert, R., J. Goldsmith, J. M. Veerbeek, J. W. Krakauer, and A. R. Luft, 2019, What the Proportional Recovery Rule Is (and Is Not): Methodological and Statistical Considerations: Neurorehabil Neural Repair, v. 33, p. 876-887.

Kwakkel, G., J. M. Veerbeek, E. E. van Wegen, and S. L. Wolf, 2015, Constraint-induced movement therapy after stroke: Lancet Neurol, v. 14, p. 224-34.

Labat-gest, V., and S. Tomasi, 2013, Photothrombotic ischemia: a minimally invasive and reproducible photochemical cortical lesion model for mouse stroke studies: J Vis Exp.

Lagace, D. C., M. C. Whitman, M. A. Noonan, J. L. Ables, N. A. DeCarolis, A. A. Arguello, M. H. Donovan, S. J. Fischer, L. A. Farnbauch, R. D. Beech, R. J. DiLeone, C. A. Greer, C. D. Mandyam, and A. J. Eisch, 2007, Dynamic contribution of nestin-expressing stem cells to adult neurogenesis: J Neurosci, v. 27, p. 12623-9.

Langhorne, P., J. Bernhardt, and G. Kwakkel, 2011, Stroke rehabilitation: The Lancet (British edition), v. 377, p. 1693-1702.

Lee, H. H., D. Y. Kim, M. K. Sohn, Y.-I. Shin, G.-J. Oh, Y.-S. Lee, M. C. Joo, S. Y. Lee, J. Han, J. Ahn, W. H. Chang, I. Kim, S. Mi Choi, J. Lee, and Y.-H. Kim, 2021, Revisiting the Proportional Recovery Model in View of the Ceiling Effect of Fugl-Meyer Assessment: Stroke (1970), v. 52, p. 3167-3175.

Lim, D. H., J. M. LeDue, M. H. Mohajerani, and T. H. Murphy, 2014, Optogenetic mapping after stroke reveals network-wide scaling of functional connections and heterogeneous recovery of the peri-infarct: J Neurosci, v. 34, p. 16455-66.

Lindsay, M., G. Gubitz, M. Bayley, S. Phillips, and E. Smith, 2014, CANADIAN STROKE BEST PRACTICE RECOMMENDATIONS.

Mansoori, B. K., L. Jean-Charles, B. Touvykine, A. Liu, S. Quessy, and N. Dancause, 2014, Acute inactivation of the contralesional hemisphere for longer durations improves recovery after cortical injury: Experimental neurology, v. 254, p. 18-28.

Mathis, A., P. Mamidanna, K. M. Cury, T. Abe, V. N. Murthy, M. W. Mathis, and M. Bethge, 2018, DeepLabCut: markerless pose estimation of user-defined body parts with deep learning: Nat Neurosci, v. 21, p. 1281-1289.

Mathis, A., S. Schneider, J. Lauer, and M. W. Mathis, 2020, A Primer on Motion Capture with Deep Learning: Principles, Pitfalls, and Perspectives: Neuron, v. 108, p. 44-65.

McPhail, L. T., C. B. McBride, J. McGraw, J. D. Steeves, and W. Tetzlaff, 2004, Axotomy abolishes NeuN expression in facial but not rubrospinal neurons: Experimental neurology, v. 185, p. 182-190.

Minatohara, K., M. Akiyoshi, and H. Okuno, 2015, Role of Immediate-Early Genes in Synaptic Plasticity and Neuronal Ensembles Underlying the Memory Trace: Frontiers in molecular neuroscience, v. 8, p. 78-78.

Mohajerani, M. H., K. Aminoltejari, and T. H. Murphy, 2011, Targeted mini-strokes produce changes in interhemispheric sensory signal processing that are indicative of disinhibition within minutes: Proc Natl Acad Sci U S A, v. 108, p. E183-91.

Nath, T., A. Mathis, A. C. Chen, A. Patel, M. Bethge, and M. W. Mathis, 2019, Using DeepLabCut for 3D markerless pose estimation across species and behaviors: Nat Protoc, v. 14, p. 2152-2176.

Nikolaienko, O., S. Patil, M. S. Eriksen, and C. R. Bramham, 2018, Arc protein: a flexible hub for synaptic plasticity and cognition: Seminars in cell & developmental biology, v. 77, p. 33-42.

NINDS, 2022a, Optimizing endovascular therapy for ischemic stroke, NINDS Contributions to Approved Therapies, Online, National Institute of Neurological Disorders and Stroke.

NINDS, 2022b, Tissue Plasminogen Activator for Acute Ischemic Stroke (Alteplase, Activase®), NINDS Contributions to Approved Therapies, Online, National Institute of Neurological Disorders and Stroke.

Nishimura, Y., H. Onoe, Y. Morichika, S. Perfiliev, H. Tsukada, and T. Isa, 2007, Time-dependent central compensatory mechanisms of finger dexterity after spinal cord injury: Science, v. 318, p. 1150-5.

Olafson, E. R., K. W. Jamison, E. M. Sweeney, H. Liu, D. Wang, J. E. Bruss, A. D. Boes, and A. Kuceyeski, 2021, Functional connectome reorganization relates to post-stroke motor recovery and structural and functional disconnection: Neuroimage, v. 245, p. 118642.

Pascual, K. J., E. Vlasova, K. J. Lockett, J. Richardson, and M. Yochelson, 2018, Evaluating the Impact of Personalized Stroke Management Tool Kits on Patient Experience and Stroke Recovery: Journal of patient experience, v. 5, p. 244-249.

Prabhakaran, S., E. Zarahn, C. Riley, A. Speizer, J. Y. Chong, R. M. Lazar, R. S. Marshall, and J. W. Krakauer, 2008, Inter-individual Variability in the Capacity for Motor Recovery After Ischemic Stroke: Neurorehabilitation and neural repair, v. 22, p. 64-71.

Rehme, A. K., S. B. Eickhoff, C. Rottschy, G. R. Fink, and C. Grefkes, 2012, Activation likelihood estimation meta-analysis of motor-related neural activity after stroke: Neuroimage, v. 59, p. 2771-82.

Rehme, A. K., G. R. Fink, D. Y. von Cramon, and C. Grefkes, 2011, The role of the contralesional motor cortex for motor recovery in the early days after stroke assessed with longitudinal FMRI: Cereb Cortex, v. 21, p. 756-68.

Rodríguez, J. J., H. A. Davies, M. L. Errington, A. Verkhratsky, T. V. P. Bliss, and M. G. Stewart, 2008, ARG3.1/ARC expression in hippocampal dentate gyrus astrocytes: ultrastructural evidence and co-localization with glial fibrillary acidic protein: Journal of cellular and molecular medicine, v. 12, p. 671-678.

Rogers, J. M., J. Duckworth, S. Middleton, B. Steenbergen, and P. H. Wilson, 2019, Elements virtual rehabilitation improves motor, cognitive, and functional outcomes in adult stroke: evidence from a randomized controlled pilot study: J Neuroeng Rehabil, v. 16, p. 56.

Rymer, M. M., 2011, Hemorrhagic stroke: intracerebral hemorrhage: Missouri medicine, v. 108, p. 50-54.

Sigler, A., M. H. Mohajerani, and T. H. Murphy, 2009, Imaging rapid redistribution of sensory-evoked depolarization through existing cortical pathways after targeted stroke in mice: Proc Natl Acad Sci U S A, v. 106, p. 11759-64.

Smith, M. C., W. D. Byblow, P. A. Barber, and C. M. Stinear, 2017, Proportional Recovery From Lower Limb Motor Impairment After Stroke: Stroke, v. 48, p. 1400-1403.

Smith, W. S., G. Sung, S. Starkman, J. L. Saver, C. S. Kidwell, Y. P. Gobin, H. L. Lutsep, G. M. Nesbit, T. Grobelny, M. M. Rymer, I. E. Silverman, R. T. Higashida, R. F. Budzik, and M. P. Marks, 2005, Safety and efficacy of mechanical embolectomy in acute ischemic stroke: results of the MERCI trial: Stroke (1970), v. 36, p. 1432-1438.

Takatsuru, Y., D. Fukumoto, M. Yoshitomo, T. Nemoto, H. Tsukada, and J. Nabekura, 2009, Neuronal circuit remodeling in the contralateral cortical hemisphere during functional recovery from cerebral infarction: J Neurosci, v. 29, p. 10081-6.

Tom Curran, A., D. Miller, L. Zokas, and I. M. Verma, 1984, Viral and cellular fos proteins: A comparative analysis: Cell, v. 36, p. 259-268.

Tombari, D., I. Loubinoux, J. Pariente, A. Gerdelat, J. F. Albucher, J. Tardy, E. Cassol, and F. Chollet, 2004, A longitudinal fMRI study: in recovering and then in clinically stable sub-cortical stroke patients: Neuroimage, v. 23, p. 827-39.

van der Vliet, R., R. Selles, E. Aninopoulou, R. Nijland, G. Ribbers, M. Frens, C. Meskers, and G. Kwakkel, 2020, Predicting Upper Limb Motor Impairment Recovery after Stroke: A Mixture Model: Annals of neurology, v. 87, p. 383-393.

Vani, M., 2018, Establishing a Model to Label and Stimulate Cells Active During Motor Behaviour, uOttawa, https://ruor.uottawa.ca/handle/10393/38066.

Veronika, K., K. Diarmuid, M. J. Richardson, and D. M. Kaplan, 2022, Validation of DeepLabCut as a tool for markerless 3D pose estimation, bioRxiv.

Wahl, A. S., W. Omlor, J. C. Rubio, J. L. Chen, H. Zheng, A. Schroter, M. Gullo, O. Weinmann, K. Kobayashi, F. Helmchen, B. Ommer, and M. E. Schwab, 2014, Neuronal repair. Asynchronous therapy restores motor control by rewiring of the rat corticospinal tract after stroke: Science, v. 344, p. 1250-5.

Ward, N. S., M. M. Brown, A. J. Thompson, and R. S. Frackowiak, 2003, Neural correlates of motor recovery after stroke: a longitudinal fMRI study: Brain, v. 126, p. 2476-96.

Weiller, C., F. Chollet, K. J. Friston, R. J. Wise, and R. S. Frackowiak, 1992, Functional reorganization of the brain in recovery from striatocapsular infarction in man: Ann Neurol, v. 31, p. 463-72.

WHO, 2020, The top 10 causes of death, *in* W. H. Organization, ed., WHO's Global Health Estimates, Online, World Health Organization.

Williamson, M. R., T. A. Jones, and M. R. Drew, 2019, Functions of subventricular zone neural precursor cells in stroke recovery: Behavioural brain research, v. 376, p. 112209-112209.

Wu, K.-L., Y.-Q. Li, A. Tabassum, W.-Y. Lu, I. Aubert, and C. S. Wong, 2010, Loss of Neuronal Protein Expression in Mouse Hippocampus After Irradiation: Journal of neuropathology and experimental neurology, v. 69, p. 272-280.

Xing, P. F., P. F. Yang, Z. F. Li, L. Zhang, H. J. Shen, Y. X. Zhang, Y. W. Zhang, and J. M. Liu, 2020, Comparison of Aspiration versus Stent Retriever Thrombectomy as the Preferred Strategy for Patients with Acute Terminal Internal Carotid Artery Occlusion: A Propensity Score Matching Analysis: American journal of neuroradiology : AJNR, v. 41, p. 469-476.

Ye, L., W. E. Allen, K. R. Thompson, Q. Tian, B. Hsueh, C. Ramakrishnan, A. C. Wang, J. H. Jennings, A. Adhikari, C. H. Halpern, I. B. Witten, A. L. Barth, L. Luo, J. A. McNab, and K. Deisseroth, 2016, Wiring and Molecular Features of Prefrontal Ensembles Representing Distinct Experiences: Cell, v. 165, p. 1776-1788.

Zeiger, W. A., M. Marosi, S. Saggi, N. Noble, I. Samad, and C. Portera-Cailliau, 2021, Barrel cortex plasticity after photothrombotic stroke involves potentiating responses of pre-existing circuits but not functional remapping to new circuits: Nat Commun, v. 12, p. 3972.

Zukin, R. S., T. Jover, H. Yokota, A. Calderone, M. Simionescu, and C. G. Lau, 2004, Molecular and Cellular Mechanisms of Ischemia-Induced Neuronal Death, Elsevier Inc., 829-854 p.